

# ‘Universal’ microstructural patterns in cortical and trabecular, extracellular and extravascular bone materials: Micromechanics-based prediction of anisotropic elasticity

Andreas Fritsch<sup>1</sup>, Christian Hellmich\*

*Institute for Mechanics of Materials and Structures, Vienna University of Technology (TU Wien), A-1040 Vienna, Austria*

Received 17 March 2006; received in revised form 6 September 2006; accepted 8 September 2006

Available online 17 September 2006

## Abstract

Bone materials are characterized by an astonishing variability and diversity. Still, because of ‘architectural constraints’ due to once chosen material constituents and their physical interaction, the fundamental hierarchical organization or basic building plans of bone materials remain largely unchanged during biological evolution. Such universal patterns of microstructural organization govern the mechanical interaction of the elementary components of bone (hydroxyapatite, collagen, water; with directly measurable tissue-independent elastic properties), which are here quantified through a multiscale homogenization scheme delivering effective elastic properties of bone materials: at a scale of 10 nm, long cylindrical collagen molecules, attached to each other at their ends by ~1.5 nm long crosslinks and hosting intermolecular water inbetween, form a contiguous matrix called wet collagen. At a scale of several hundred nanometers, wet collagen and mineral crystal agglomerations interpenetrate each other, forming the mineralized fibril. At a scale of 5–10  $\mu\text{m}$ , the extracellular solid bone matrix is represented as collagen fibril inclusions embedded in a foam of largely disordered (extrafibrillar) mineral crystals. At a scale above the ultrastructure, where lacunae are embedded in extracellular bone matrix, the extravascular bone material is observed. Model estimates predicted from tissue-specific composition data gained from a multitude of chemical and physical tests agree remarkably well with corresponding acoustic stiffness experiments across a variety of cortical and trabecular, extracellular and extravascular materials. Besides from reconciling the well-documented, seemingly opposed concepts of ‘mineral-reinforced collagen matrix’ and ‘collagen-reinforced mineral matrix’ for bone ultrastructure, this approach opens new possibilities in the exploitation of computer tomographic data for nano-to-macro mechanics of bone organs.

© 2006 Elsevier Ltd. All rights reserved.

**Keywords:** Bone; Universal microstructural patterns; Continuum micromechanics; Anisotropy; Elasticity; Hydroxyapatite; Collagen; Fibril; Lacunae

## 1. Introduction

Bone materials are characterized by an astonishing variability and diversity. Their hierarchical organizations are often well suited and seemingly optimized to fulfill specific mechanical functions. This has motivated research in the fields of bionics and biomimetics. The aforemen-

tioned optimization is primarily driven by selection during the biological evolution process. However, apart from the fact that selection is quite unlikely to push bone skeletal and material design to a well-defined optimum (Nowlan and Prendergast, 2005), it is of great importance to notice that selection is realized at the level of the individual plant or animal (and not at the material level). Therefore, material optimization in the strictest sense of the word does not take place. Rather, ‘architectural constraints’ (Seilacher, 1970; Gould and Lewontin, 1979) merely due to once chosen material constituents and their physical interactions imply the fundamental hierarchical organization patterns or basic building plans, which remain largely unchanged during biological evolution. Firstly, these building plans

\*Corresponding author. Tel.: +43 15880120220;  
fax: +43 15880120299.

E-mail addresses: [Andreas.Fritsch@tuwien.ac.at](mailto:Andreas.Fritsch@tuwien.ac.at) (A. Fritsch),  
[Christian.Hellmich@tuwien.ac.at](mailto:Christian.Hellmich@tuwien.ac.at) (C. Hellmich).

<sup>1</sup>Present address: Laboratoire des Matériaux et des Structures du Génie Civil, Ecole Nationale des Ponts et Chaussées, 77455 Marne-la-Vallée, France.

are expressed by typical morphological features which can be discerned across all bone materials. Katz et al. (1984) distinguish five levels of hierarchical organization, which have been quite generally accepted in the scientific community:

- The macrostructure at an observation scale of several mm to cm, where cortical (or compact) bone and trabecular (or spongy) bone can be distinguished [Fig. 1(a) and (b)];
- The microstructure at an observation scale of several 100  $\mu\text{m}$  to several mm, where cylindrical units called osteons build up cortical bone, and where the single trabecular struts or plates can be distinguished [Fig. 1(c) and (d)];
- The ultrastructure (or extracellular solid bone matrix) at an observation scale of several  $\mu\text{m}$ , comprising the material building up both trabecular struts and osteons [Fig. 1(e)].
- Within the ultrastructure, collagen-rich domains [light areas in Fig. 1(e)] and collagen-free domains [dark areas in Fig. 1(e)] can be distinguished at an observation scale of several hundred nanometers. Commonly, these domains are referred to as fibrils and extrafibrillar space.
- Finally, at an observation scale of several ten nanometers, the so-called elementary components of mineralized tissues can be distinguished. These are:
  - Plate-shaped mineral crystals consisting of impure hydroxyapatite (HA;  $\text{Ca}_{10}[\text{PO}_4]_6[\text{OH}]_2$ ) with typical 1–5 nm thickness, and 25–50 nm length (Weiner and Wagner, 1998) [Fig. 1(f)].

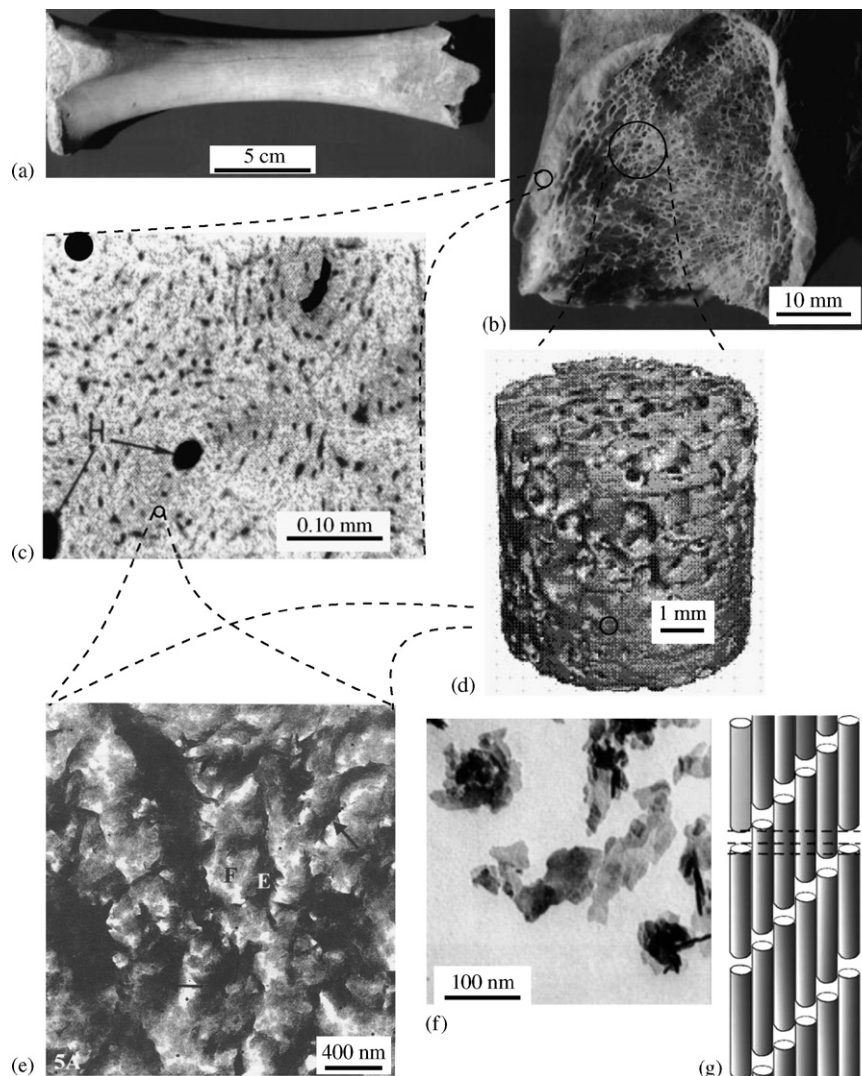


Fig. 1. Hierarchical organization of bone: (a) whole long bone (macrostructure)(+); (b) section through long bone (macrostructure)(+); (c) osteonal cortical bone (microstructure)(o); (d) trabecular spaceframe (microstructure)(□); (e) ultrastructure(×); (f) hydroxyapatite crystals (elementary components)(+); (g) collagen molecules (elementary components)(+); (+) ... from (Weiner and Wagner, 1998), reprinted, with permission, from the Annual Review of Materials Science, Vol. 28 (c)1998 by Annual Reviews, [www.AnnualReviews.org](http://www.AnnualReviews.org); (o) ... reused with permission from Sidney Lees, Paul F. Cleary, John D. Heeley, and Ernest L. Garipey, The Journal of the Acoustical Society of America, 66, 641 (1979). (c) 1979, Acoustical Society of America; (□) ... Reprinted from (Ding and Hvid, 2000), with permission from Elsevier; (×) ... from (Prostak and Lees, 1996), p.478, Fig. 5a, with kind permission of Springer Science and Business Media.

- Long cylindrically shaped collagen molecules with a diameter of about 1.2 nm and a length of about 300 nm (Lees, 1987), which are self-assembled in staggered organizational schemes (fibrils) with characteristic diameters of 50–500 nm (Cusack and Miller, 1979; Miller, 1984; Lees et al., 1990, 1994b; Weiner et al., 1997; Weiner and Wagner, 1998; Rho et al., 1998; Probst and Lees, 1996), [Fig. 1(g)]; several covalently bonded fibrils are sometimes referred to as fibers.
- Different non-collagenous organic molecules, predominantly lipids and proteins (Urist et al., 1983; Hunter et al., 1996) and
- Water.

Secondly, the aforementioned universal microstructural patterns across the hierarchical organization of bone concern the mechanical interaction between the elementary components, governing the elasticity of the material at all different observation scales, as was probably first pointed out by Katz (1980). In the open literature, there is no general agreement on the interaction of collagen and mineral: The concept of a ‘mineral-reinforced collagen matrix’ (Currey, 1969; Katz, 1980, 1981; Sasaki, 1991; Mammone and Hudson, 1993; Jäger and Fratzl, 2000; Kotha and Guzelsu, 2003) is seemingly opposed to that of a mineral matrix with collagen inclusions (Crolet et al., 1993; Aoubiza et al., 1996; Benezra Rosen et al., 2002; Hellmich and Ulm, 2002a; Wang and Qian, 2006).

The collagen matrix introduced in the first concept does not refer to molecular collagen with a stiffness of several GPa (Harley et al., 1977; Cusack and Miller, 1979; Sasaki and Odajima 1996a, b; Lorenzo and Caffarena, 2005; Vesentini et al., 2005), but to a ‘collagen–water composite’ or ‘wet collagen’, with significantly smaller stiffness. However, there is no general agreement either on the magnitude of this stiffness: experiments reveal a few MPa stiffness for collagen fibrils self-assembling under laboratory conditions (Christiansen et al., 2000), several tens of MPa stiffness for unmineralized turkey leg tendon (Landis et al., 1995; used in the model of Jäger and Fratzl, 2000), several hundreds of MPa for demineralized bone (Bowman et al., 1996; Catanese et al., 1999), and 1.5 GPa for leather-type skin (Hall, 1951; used in the models of Currey, 1969; Katz, 1980, 1981; Sasaki, 1991; Mammone and Hudson, 1993).

As regards the second concept, recent research work strongly suggests the ‘mineral matrix’ to be a mineral foam or porous polycrystal with typically several nm-sized water-filled ‘nano-pores’. This recent research work comprises material science contributions (Benezra Rosen et al., 2002), cellular solid-type mechanical energy considerations (Hellmich and Ulm, 2002a) relying on a comprehensive experimental data base encompassing the pioneering work of Lees et al. (1983); Lees (1987); Lees et al. (1994a, 1995), and continuum micromechanics models (Hellmich and Ulm, 2002b; Hellmich et al., 2004a; Fritsch et al., 2006).

A central issue of this paper is that probably both concepts are relevant for the mineral–collagen interaction in the bone ultrastructure, but clearly at *different* observation scales: in the line of the ‘mineral-reinforced collagen matrix’-concept we consider, at an observation scale of some tens of nanometers, a ‘collagen matrix material’ called ‘wet collagen’, consisting of 1.2 nm thick collagen molecules and intermolecular water. At a scale of several hundred nanometers, we envision the mineralized collagen fibril to be formed by wet collagen and by mineral crystal agglomerations, interpenetrating each other. At a scale of 5–10  $\mu\text{m}$ , however, the mineralized collagen fibrils themselves are embedded in an extrafibrillar mineral foam, in the line of the concept of a ‘mineral matrix with collagen inclusions’.

For relating the aforementioned vision of ultrastructural organization to effective elastic properties, we rely on homogenization theory (continuum micromechanics, Hill, 1963; Suquet, 1997; Zaoui, 1997, see Section 2), which is a well-established tool for structure–property investigations of bone or teeth, both at the microstructural level (Katz, 1980, 1981; Sevostianov and Kachanov, 2000; Hellmich et al., 2004b; Qin and Swain, 2004; Hellmich, 2005; Huo, 2005), and at the ultrastructural level (Hellmich and Ulm, 2002b; Hellmich et al., 2004a). Thereby, we invest into careful validation of our micromechanical development (described in Section 3) through independent experiments related to (i) the elasticity of the elementary components, and to (ii) composition and elasticity of different bone tissues from different animals and different anatomical locations both at the extracellular and extravascular level (described in Section 4). Since we avoid introduction of micromorphological features which cannot be experimentally quantified (such as e.g. the ‘arrangement of lamellae’ around osteons in ‘lamellar’ cortical bone), no material parameters are left for tuning or back-analysis. Hence, the capability and the limitations of our mathematically expressed construction plan for extracellular and extravascular bone materials can be directly assessed in terms of model prediction errors. They are given in Section 4, and they are the basis for the Discussion (Section 5).

## 2. Fundamentals of continuum micromechanics—linear elasticity

In continuum micromechanics (Hill, 1963; Suquet, 1997; Zaoui, 2002), a material is understood as a macro-homogeneous, but micro-heterogeneous body filling a representative volume element (RVE) with characteristic length  $\ell$ ,  $\ell \gg d$ ,  $d$  standing for the characteristic length of inhomogeneities within the RVE (see Fig. 2), and  $\ell \ll \mathcal{L}$ ,  $\mathcal{L}$  standing for the characteristic lengths of geometry or loading of a structure built up by the material defined on the RVE. In general, the microstructure within one RVE is so complicated that it cannot be described in complete detail. Therefore, quasi-homogeneous subdomains with known physical quantities (such as volume fractions or

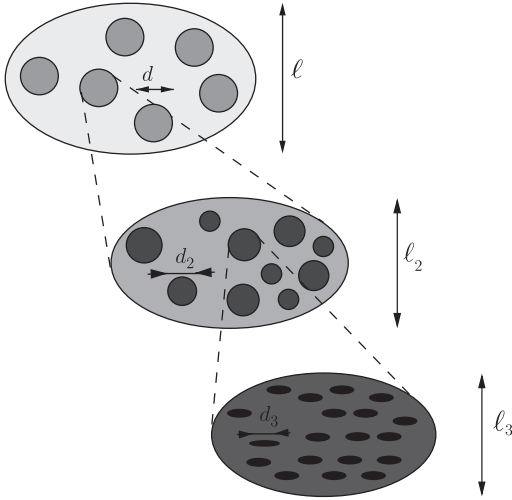


Fig. 2. Multistep homogenization.

elastic properties) are reasonably chosen. They are called material phases. The ‘homogenized’ mechanical behavior of the overall material, i.e. the relation between homogeneous deformations acting on the boundary of the RVE and resulting (average) stresses, can then be estimated from the mechanical behavior of the aforementioned homogeneous phases (representing the inhomogeneities within the RVE), their dosages within the RVE, their characteristic shapes, and their interactions. Based on matrix-inclusion problems (Eshelby, 1957; Laws, 1977), an estimate for the ‘homogenized’ stiffness of a material reads as (Zaoui, 2002)

$$\mathbb{C}^{est} = \sum_r f_r \mathbb{C}_r : [\mathbb{I} + \mathbb{P}_r^0 : (\mathbb{C}_r - \mathbb{C}^0)]^{-1} : \left\{ \sum_s f_s [\mathbb{I} + \mathbb{P}_s^0 : (\mathbb{C}_s - \mathbb{C}^0)]^{-1} \right\}^{-1}, \quad (1)$$

where  $\mathbb{C}_r$  and  $f_r$  denote the elastic stiffness and the volume fraction of phase  $r$ , respectively, and  $\mathbb{I}$  is the fourth-order unity tensor. The two sums are taken over all phases of the heterogeneous material in the RVE. The fourth-order Hill tensor  $\mathbb{P}_r^0$  accounts for the characteristic shape of phase  $r$  in a matrix with stiffness  $\mathbb{C}^0$ . Choice of this stiffness describes the interactions between the phases: for  $\mathbb{C}^0$  coinciding with one of the phase stiffnesses (Mori–Tanaka scheme, Mori and Tanaka, 1973; Wakashima and Tsukamoto, 1991), a composite material is represented (contiguous matrix with inclusions); for  $\mathbb{C}^0 = \mathbb{C}^{est}$  (self-consistent scheme (Hershey, 1954; Hill, 1963)), a dispersed arrangement of the phases is considered (typical for polycrystals). If a single phase exhibits a heterogeneous microstructure itself, its mechanical behavior can be estimated by introduction of an RVE within this phase, with dimensions  $\ell_2 \leq d$ , comprising again smaller phases with characteristic length  $d_2 \leq \ell_2$ , and so on (see Fig. 2).

This leads to a multistep homogenization scheme. Such a procedure will be applied to mammalian cortical and trabecular bone materials in the sequel.

### 3. Micromechanical representation of hierarchical organisation of bone materials

Across the hierarchical organization of bone materials, the following ‘universal’ microstructural patterns are considered in the framework of a multistep homogenization scheme (Fig. 3): the first homogenization step refers to an observation scale of several nanometers, where cross-linked collagen molecules form a contiguous matrix, which is ‘perforated’ by intermolecular, water-filled spaces. We call the homogenized material ‘wet collagen’ [Section 3.1 and Fig. 3(a)]. At the fibrillar observation scale, wet collagen and mineral crystal agglomerations penetrate each other, building up the mineralized fibril [Section 3.2 and Fig. 3(b)]. At the ultrastructural scale, mineralized fibrils are embedded as inclusions into the extrafibrillar mineral foam [Section 3.3 and Fig. 3(c), (Hellmich and Ulm, 2002a; Hellmich et al., 2004a)], forming together the extracellular bone matrix or ultrastructure [Section 3.4 and Fig. 3(d)]. The last homogenization step considered herein refers to extravascular bone material at an observation scale of  $\ell \approx 100 \mu\text{m}$  [compare bar in Fig. 1(c)], where lacunar pores are embedded in an ultrastructural matrix [Section 3.5 and Fig. 3(e)]. At an even higher observation scale, that of the microstructure with  $\ell \approx 500 \mu\text{m}$ , this extravascular matrix would be perforated by Haversian canals (in cortical bone) or by intertrabecular porosity (in trabecular bone). Material mechanics at that scale is beyond the scope of the present manuscript.

#### 3.1. Wet collagen

Within an RVE  $\hat{V}_{wetcol}$  of wet collagen with  $\ell_{wetcol} \approx 10 \text{ nm}$  characteristic length [Fig. 3(a)], we homogenize over the staggered organization of cylindrical collagen molecules [Fig. 1(g), Hodge and Petruska, 1963; Miller, 1984], which are attached to each other at their ends by  $\sim 1.5 \text{ nm}$  long crosslinks [Lees et al., 1984b; Bailey et al., 1998, see also Section 4.3, Eq. (35)ff.]. These crosslinks imply the existence of a contiguous matrix built up by molecular collagen, ‘perforated’ by intermolecular spaces. The latter are represented by cylindrical inclusions hosting water containing mechanically insignificant amounts of non-collagenous organic matter [Fig. 3(a)]. The volume fractions occupied by the two phases ‘molecular collagen’ and ‘intermolecular space’ are  $\hat{f}_{col}$  and  $\hat{f}_{im}$ ,  $\hat{f}_{col} + \hat{f}_{im} = 1$ . Using a Mori–Tanaka scheme for the estimation of the stiffness of the composite material ‘wet collagen’,  $\mathbb{C}_{wetcol}^{MT}$ , we specify (1) for one (cylindrical) inclusion phase (intermolecular water) and a matrix of molecular collagen, i.e. for  $r \in [col, im]$ , for  $\mathbb{C}_{im} = 3k_{H_2O} \mathbb{I}$ , with  $J_{ijkl} = 1/3 \delta_{ij} \delta_{kl}$  as the volumetric part of the fourth order unity tensor  $\mathbb{I}$ , and  $\mathbb{C}^0 = \mathbb{C}_{col}$  according to Table 1, as well as for



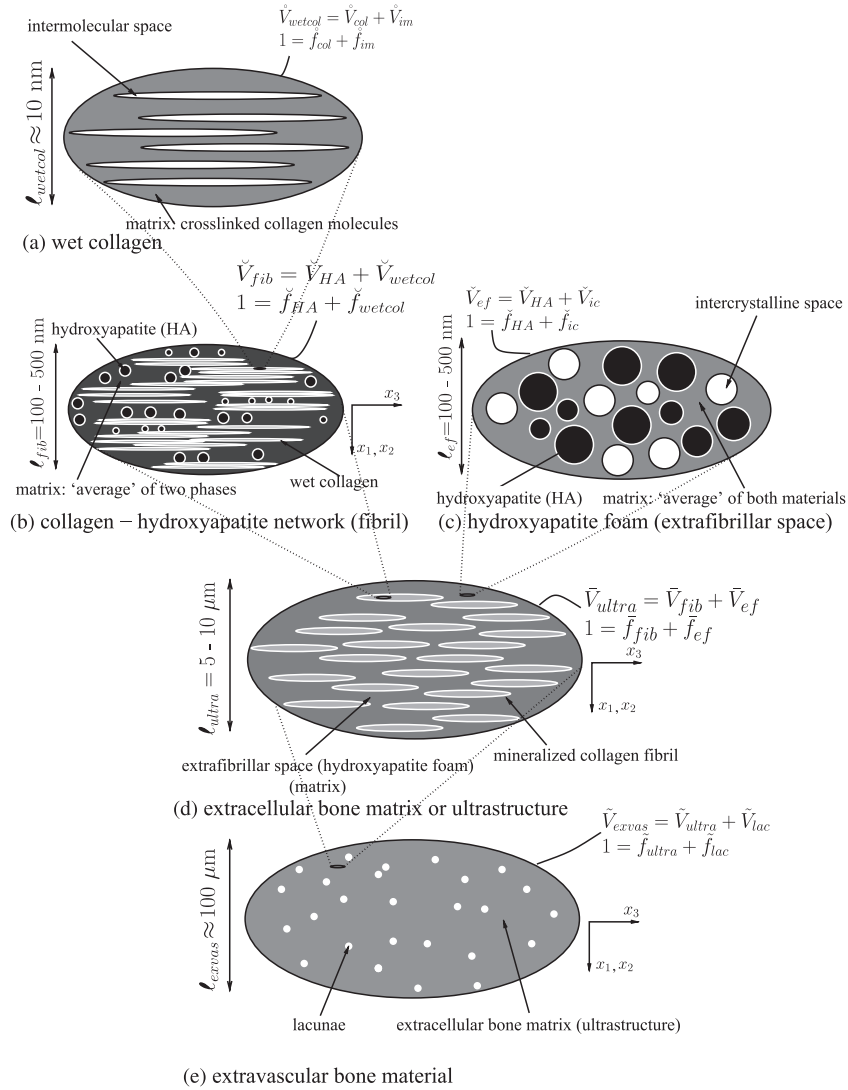


Fig. 3. Micromechanical representation of bone material by means of a five-step homogenization procedure.

Table 1

‘Universal’ (tissue and location-independent) isotropic (or transversely isotropic) phase stiffness values

| Phase  | Bulk modulus<br>$k$ [GPa]                                   | Shear modulus<br>$\mu$ [GPa]   | Experimental source        |
|--|---|--|----------------------------|
| Hydroxyapatite<br>water containing<br>non-collageneous<br>organics or osteocytes | $k_{HA} = 82.6$<br><br>$k_{H_2O} = 2.3$<br>$c_{ijkl}$ [GPa] | $\mu_{HA} = 44.9$<br><br>$\mu_{H_2O} = 0$<br>$c_{ijkl}$ [GPa]        | (Katz and Ukraincik, 1971) |
| Collagen   | $c_{col,3333} = 17.9$<br>$c_{col,1111} = 11.7$              | $c_{col,1133} = 7.1$<br>$c_{col,1122} = 5.1$<br>$c_{col,1313} = 3.3$ | (Cusack and Miller, 1979)  |

 $\mathbb{P}_{im}^0 = \mathbb{P}_{cyl}^{col}$ , resulting in

$$\mathbb{C}_{wetcol}^{MT} = \{(1 - \hat{f}_{im})\mathbb{C}_{col} + \hat{f}_{im}\mathbb{C}_{im} : [\mathbb{I} + \mathbb{P}_{cyl}^{col} : (\mathbb{C}_{im} - \mathbb{C}_{col})]^{-1}\} : \{(1 - \hat{f}_{im})\mathbb{I} + \hat{f}_{im}[\mathbb{I} + \mathbb{P}_{cyl}^{col} : (\mathbb{C}_{im} - \mathbb{C}_{col})]^{-1}\}^{-1}. \quad (2)$$

$\mathbb{C}_{wetcol}^{MT}$  possesses an axis of rotational symmetry, the material is transversely isotropic.  $\mathbb{P}_{cyl}^{col}$  refers to a cylindrical inclusion in a transversely isotropic matrix with stiffness  $\mathbb{C}_{col}$ , where the plane of isotropy is oriented perpendicular to the long axis of the cylinder. The non-zero components

of the symmetric tensor  $\mathbb{P}_{cyl}^{col}$  read as follows (Hellmich et al., 2004a; Levin et al., 2000):

$$P_{cyl,1111}^{col} = P_{cyl,2222}^{col} = 1/8(5c_{col,1111} - 3c_{col,1122})/c_{col,1111}/\mathcal{D}_2, \quad (3)$$

$$P_{cyl,1122}^{col} = P_{cyl,2211}^{col} = -1/8(c_{col,1111} + c_{col,1122})/c_{col,1111}/\mathcal{D}_2, \quad (4)$$

$$P_{cyl,2323}^{col} = P_{cyl,1313}^{col} = 1/(8c_{col,2323}), \quad (5)$$

$$P_{cyl,1212}^{col} = 1/8(3c_{col,1111} - c_{col,1122})/c_{col,1111}/\mathcal{D}_2 \quad (6)$$

whereby

$$\mathcal{D}_2 = c_{col,1111} - c_{col,1122}. \quad (7)$$

### 3.2. Mineralized collagen fibril

Within an RVE  $\check{V}_{fib}$  of fibrillar material [Fig. 3(b)] with characteristic length of  $\ell_{fib} = 100\text{--}500\text{ nm}$  (Cusack and Miller, 1979; Miller, 1984; Probst and Lees, 1996), the phases ‘hydroxyapatite (HA)’ and ‘wet collagen’ occupy volume fractions  $\check{f}_{HA}$  and  $\check{f}_{wetcol}$ ,  $\check{f}_{HA} + \check{f}_{wetcol} = 1$ . The crystals form agglomerations of typical size  $d_{HA} \approx 10\text{ nm}$  (Landis et al., 1996), filling (during the mineralization process) the gap zones in the collagen fibrils, before spreading through the fibrils. Both phases interpenetrate each other, which motivates the use of a self-consistent scheme, with spherical inclusions for the mineral phase, and with cylindrical inclusions for the wet collagen phase. Accordingly, in order to estimate the stiffness of the mineralized collagen fibril,  $\mathbb{C}_{fib}^{SCS}$ , (1) is specified for one spherical inclusion phase (mineral) and one cylindrical inclusion phase (wet collagen), i.e. for  $r \in [HA, wetcol]$ , for  $\mathbb{C}_{HA} = 3k_{HA}\mathbb{J} + 2\mu_{HA}\mathbb{K}$  ( $\mathbb{K} = \mathbb{I} - \mathbb{J}$  is the deviatoric part of the fourth-order unity tensor  $\mathbb{I}$ ) according to Table 1, and for  $\mathbb{C}_{wetcol} = \mathbb{C}_{wetcol}^{MT}$  from (2), for  $\mathbb{C}^0 = \mathbb{C}_{fib}^{SCS}$ , as well as for  $\mathbb{P}_{HA}^0 = \mathbb{P}_{sph}^{fib}$  and  $\mathbb{P}_{wetcol}^0 = \mathbb{P}_{cyl}^{fib}$ ; resulting in

$$\begin{aligned} \mathbb{C}_{fib}^{SCS} &= \{\check{f}_{wetcol} \mathbb{C}_{wetcol}^{MT} : [\mathbb{I} + \mathbb{P}_{cyl}^{fib} : (\mathbb{C}_{wetcol}^{MT} - \mathbb{C}_{fib}^{SCS})]^{-1} \\ &\quad + \check{f}_{HA} \mathbb{C}_{HA} : [\mathbb{I} + \mathbb{P}_{sph}^{fib} : (\mathbb{C}_{HA} - \mathbb{C}_{fib}^{SCS})]^{-1} \} \\ &\quad : \{\check{f}_{wetcol} [\mathbb{I} + \mathbb{P}_{cyl}^{fib} : (\mathbb{C}_{wetcol}^{MT} - \mathbb{C}_{fib}^{SCS})]^{-1} \\ &\quad + \check{f}_{HA} [\mathbb{I} + \mathbb{P}_{sph}^{fib} : (\mathbb{C}_{HA} - \mathbb{C}_{fib}^{SCS})]^{-1} \}^{-1}. \end{aligned} \quad (8)$$

$\mathbb{C}_{fib}^{SCS}$  possesses an axis of rotational symmetry, the material is transversely isotropic. The non-zero components of  $\mathbb{P}_{cyl}^{fib}$  follow from substitution of ‘ $c_{col,ijkl}$ ’ by ‘ $C_{fib,ijkl}^{SCS}$ ’ in (3)–(7). The non-zero components of  $\mathbb{P}_{sph}^{fib}$  follow from substitution of ‘ $C_{ijkl}^0$ ’ by ‘ $C_{fib,ijkl}^{SCS}$ ’ in Eq. (A.1)–(A.7), see Appendix. For implicit solution of (8), we refer to (Hellmich et al., 2004a).

### 3.3. Extrafibrillar space: hydroxyapatite foam

Within an RVE  $\check{V}_{ef}$  of hydroxyapatite foam with  $\ell_{ef} = 100\text{--}500\text{ nm}$  characteristic length [see Fig. 3(c)], the phases ‘hydroxyapatite (HA)’ with  $d_{HA} = 1\text{--}10\text{ nm}$  (Fratzl et al., 1991; Lees et al., 1994b; Eppell et al., 2001) and ‘intercrystalline space (ic)’ occupy volume fractions  $\check{f}_{HA}$  and  $\check{f}_{ic}$ ,  $\check{f}_{HA} + \check{f}_{ic} = 1$ . The considerable disorder of the hydroxyapatite crystals in the foam, shown by Lees et al. (1994b); Fratzl et al. (1996); Peters et al. (2000); Eppell (2001); Benezra Rosen et al. (2002); Hellmich and Ulm (2002a), motivates the use of a self-consistent scheme with inclusions of spherical shape (Hellmich and Ulm, 2002b; Hellmich et al., 2004a). Accordingly, in order to estimate the stiffness of the extrafibrillar mineral foam,  $\mathbb{C}_{ef}^{SCSII}$ , (1) is specified for two (spherical) inclusion phases, i.e. for  $r \in [HA, ic]$ , for  $\mathbb{C}_{HA} = 3k_{HA}\mathbb{J} + 2\mu_{HA}\mathbb{K}$  and  $\mathbb{C}_{ic} = 3k_{H_2O}\mathbb{J}$ , according to Table 1, for  $\mathbb{C}^0 = \mathbb{C}_{ef}^{SCSII}$ , and for  $\mathbb{P}_{HA}^0 = \mathbb{P}_{ic}^0 = \mathbb{P}_{sph}^{ef}$ ; resulting in

$$\begin{aligned} \mathbb{C}_{ef}^{SCSII} &= \left\{ \sum_r \check{f}_r \mathbb{C}_r : [\mathbb{I} + \mathbb{P}_{sph}^{ef} : (\mathbb{C}_r - \mathbb{C}_{ef}^{SCSII})]^{-1} \right\} \\ &\quad : \left\{ \sum_s \check{f}_s [\mathbb{I} + \mathbb{P}_{sph}^{ef} : (\mathbb{C}_s - \mathbb{C}_{ef}^{SCSII})]^{-1} \right\}^{-1}, \end{aligned} \quad (9)$$

$r, s \in [HA, ic]$ .

$\mathbb{C}_{ef}^{SCSII}$  possesses complete symmetry, the material is isotropic.  $\mathbb{P}_{sph}^{ef}$ , the Hill tensor for a spherical inclusion in an isotropic matrix of stiffness  $\mathbb{C}_{ef}^{SCSII}$ , is of the form (Eshelby, 1957; Zaoui, 1997):

$$\mathbb{P}_{sph}^{ef} = \mathbb{S}_{sph}^{Esh,ef} : \mathbb{C}_{ef}^{SCSII,-1}, \quad (10)$$

$$\mathbb{S}_{sph}^{Esh,ef} = \alpha_{ef}^{SCSII} \mathbb{J} + \beta_{ef}^{SCSII} \mathbb{K} \quad (11)$$

with

$$\begin{aligned} \alpha_{ef}^{SCSII} &= \frac{3k_{ef}^{SCSII}}{3k_{ef}^{SCSII} + 4\mu_{ef}^{SCSII}}, \\ \beta_{ef}^{SCSII} &= \frac{6(k_{ef}^{SCSII} + 2\mu_{ef}^{SCSII})}{5(3k_{ef}^{SCSII} + 4\mu_{ef}^{SCSII})}. \end{aligned} \quad (12)$$

For implicit solution of (9), together with (10)–(12), with respect to  $\mathbb{C}_{ef}^{SCSII}$ , we refer to (Hellmich and Ulm, 2002b; Hellmich et al., 2004a).

### 3.4. Extracellular bone matrix or ultrastructure

Within an RVE  $\check{V}_{ultra}$  of bone ultrastructure with  $\ell_{ultra} = 5\text{--}10\text{ }\mu\text{m}$  characteristic length [see Fig. 3(d)], cylindrical fibrillar inclusions are embedded in a contiguous matrix built up by the mineral foam material of homogenization step III (9). The volume fractions occupied by the two phases ‘mineralized collagen fibril’ and ‘extrafibrillar space’ are  $\check{f}_{fib}$  and  $\check{f}_{ef}$ ,  $\check{f}_{fib} + \check{f}_{ef} = 1$ . Using a Mori–Tanaka

scheme for the estimation of the stiffness of the composite material ‘extracellular bone matrix or ultrastructure’,  $\mathbb{C}_{ultra}^{MTII}$ , we specify (1) for one (cylindrical) inclusion phase (mineralized collagen fibrils), and one extrafibrillar matrix, i.e. for  $r \in [fib, ef]$ , for  $\mathbb{C}_{fib} = \mathbb{C}_{fib}^{SCS}$  from (8), for  $\mathbb{C}^0 = \mathbb{C}_{ef} = \mathbb{C}_{ef}^{SCSII}$  from (9), and for  $\mathbb{P}_{fib}^0 = \mathbb{P}_{cyl}^{ef}$ ; resulting in

$$\begin{aligned} \mathbb{C}_{ultra}^{MTII} = & \{ (1 - \tilde{f}_{fib}) \mathbb{C}_{ef}^{SCSII} + \tilde{f}_{fib} \mathbb{C}_{fib}^{SCS} : [\mathbb{I} + \mathbb{P}_{cyl}^{ef} \\ & : (\mathbb{C}_{fib}^{SCS} - \mathbb{C}_{ef}^{SCSII})^{-1}] : \{ (1 - \tilde{f}_{fib}) \mathbb{I} + \tilde{f}_{fib} [\mathbb{I} + \mathbb{P}_{cyl}^{ef} \\ & : (\mathbb{C}_{fib}^{SCS} - \mathbb{C}_{ef}^{SCSII})^{-1}]^{-1} \}. \end{aligned} \quad (13)$$

$\mathbb{C}_{ultra}^{MTII}$  possesses an axis of rotational symmetry, the material is transversely isotropic. The non-zero components of  $\mathbb{P}_{cyl}^{ef}$  follow from substitution of ‘ $c_{col,ijkl}$ ’ by ‘ $C_{ef,ijkl}^{SCS}$ ’ in (3)–(7).

### 3.5. Extravascular bone material

Within an RVE  $\tilde{V}_{exvas}$  of extravascular bone material with  $\ell_{exvas} \approx 100 \mu\text{m}$  characteristic length [see Fig. 3(e)], osteocyte-filled cavities called lacunae with characteristic length  $d_{lac} = 5\text{--}15 \mu\text{m}$ , Fig. 2.1 and 2.14 of (Martin et al., 1998), are embedded in a contiguous matrix built up by the extracellular bone material of homogenization step IV (13). The volume fractions occupied by the two phases ‘extracellular bone matrix (ultrastructure)’ and ‘lacunae’ are  $\tilde{f}_{ultra}$  and  $\tilde{f}_{lac}$ ,  $\tilde{f}_{ultra} + \tilde{f}_{lac} = 1$ . Using again the Mori–Tanaka scheme for the estimation of the stiffness of the composite ‘extravascular bone material’,  $\mathbb{C}_{exvas}^{MTIII}$ , we specify (1) for one spherical inclusion phase (lacunae), and one extracellular bone matrix, i.e. for  $r \in [ultra, lac]$ , for  $\mathbb{C}_{lac} = 3k_{H_2O} \mathbb{J}$  (Table 1), for  $\mathbb{C}^0 = \mathbb{C}_{ultra} = \mathbb{C}_{ultra}^{MTII}$  from (13), and for  $\mathbb{P}_{lac}^0 = \mathbb{P}_{sph}^{ultra}$ ; resulting in

$$\begin{aligned} \mathbb{C}_{exvas}^{MTIII} = & \{ \tilde{f}_{ultra} \mathbb{C}_{ultra}^{MTII} + \tilde{f}_{lac} \mathbb{C}_{lac} : [\mathbb{I} + \mathbb{P}_{sph}^{ultra} : (\mathbb{C}_{lac} - \mathbb{C}_{ultra}^{MTII})^{-1}] : \\ & : \{ \tilde{f}_{ultra} \mathbb{I} + \tilde{f}_{lac} [\mathbb{I} + \mathbb{P}_{sph}^{ultra} : (\mathbb{C}_{lac} - \mathbb{C}_{ultra}^{MTII})^{-1}]^{-1} \}. \end{aligned} \quad (14)$$

$\mathbb{C}_{exvas}^{MTIII}$  possesses an axis of rotational symmetry, the material is transversely isotropic. The non-zero components of  $\mathbb{P}_{sph}^{ultra}$  follow from substitution of ‘ $C_{ijkl}^0$ ’ by ‘ $C_{ultra,ijkl}^{MTII}$ ’ in Eq. (A.1) to Eq. (A.7), see Appendix.

## 4. Validation of micromechanical model

### 4.1. Strategy

In the line of Popper, who stated that a theory—as long as it has not been falsified—will be ‘the more satisfactory the greater the severity of independent tests it survives’, cited from Mayr (1997, p. 49), the verification of the micromechanical representation of cortical and trabecular bone materials at the ultrastructural (extracellular) and the extravascular level will rest on two independent experimental sets: The stiffness values  $\mathbb{C}_{ultra}^{MTII}$  and  $\mathbb{C}_{exvas}^{MTIII}$  predicted by the micromechanical model on the basis of tissue-independent phase stiffness properties  $\mathbb{C}_{HA} = 3k_{HA} \mathbb{J} + 2\mu_{HA} \mathbb{K}$ ,  $\mathbb{C}_{col}$ ,  $k_{H_2O}$  (experimental set I,

Table 1) for tissue-specific composition data  $\tilde{f}_{lac}$ ,  $\tilde{f}_{fib}$ ,  $\tilde{f}_{HA}$ ,  $\tilde{f}_{HA}$ , and  $\tilde{f}_{col}$  (experimental set IIa, Section 4.3) are compared to corresponding experimentally determined tissue-specific stiffness values  $\mathbb{C}^{exp}$  (experimental set IIb, Section 4.4).

### 4.2. ‘Universal’ phase stiffness values—experimental set I

Concerning the tissue-independent (‘universal’) phase properties, being the same for all tissues discussed herein, we consider the following experiments: Tests with an ultrasonic interferometer coupled with a solid media pressure apparatus (Katz and Ukraincik, 1971; Gilmore and Katz, 1982) reveal the isotropic elastic properties of hydroxyapatite powder, which, in view of the largely disordered arrangement of minerals (Lees et al., 1994b; Fratzl et al., 1996; Peters et al., 2000; Hellmich and Ulm, 2002a), are considered as sufficient for the characterization of the mineral phase (Hellmich and Ulm, 2002b; Hellmich et al., 2004b). Given the absence of direct measurements of (molecular) collagen, the elastic properties of (molecular) collagen are approximated by those of dry rat tail tendon, a tissue consisting almost exclusively of collagen. By means of Brillouin light scattering, Cusack and Miller (1979) have determined the respective five independent elastic constants of a transversely isotropic material (Table 1). We assign the standard bulk modulus of water (Table 1) to phases comprising water with mechanically insignificant non-collageneous organic matter or osteocytes. In case of dry tissues, we adopt  $k_{H_2O} = 0$ .

### 4.3. Determination of tissue-specific volume fractions—experimental set IIa

Experimental validation of the five-step homogenization procedure [Eq. (2) to (14)] requires determination of the volume fractions within the five considered RVEs (Fig. 3).

As concerns the extravascular scale [Fig. 3(e)], the corresponding volume fractions were derived from measurements at a scale of one to several mm (microstructure of bone). This scale is accessible by polarized light microscopy [Fig. 1(c)], which visualizes, in cortical bone, Haversian canals and lacunae. Hence, polarized light microscopic images can be used for determination of the (microstructural) volume fractions of vascular and lacunar porosity,  $f_{vas}$  and  $f_{lac}$ , through

$$f_{vas} = \frac{\text{area of Haversian canals in field of view}}{\text{total area of field of view}}, \quad (15)$$

$$f_{lac} = \frac{\text{area of lacunae in field of view}}{\text{total area of field of view}}. \quad (16)$$

At the extravascular scale [Fig. 3(e)] the lacunar volume fraction follows to be

$$\tilde{f}_{lac} = \frac{f_{lac}}{1 - f_{vas}}, \quad (17)$$

where  $f_{vas}$  is related to the activity of osteoblasts and osteoclasts, biological cells being temporarily active in

Haversian canals and intertrabecular space, see standard textbooks such as Martin et al. (1998).  $f_{vas}$  increases under osteoclastic activity (osteoclasts resorb extracellular bone material), and  $f_{vas}$  decreases under osteoblastic activity (osteoblasts lay down osteoid, i.e. yet unmineralized bone ultrastructure, at the surfaces of Haversian canals or of trabecular plates or struts). Reflecting a certain equilibrium between osteoclastic and osteoblastic activity,  $f_{vas}$  ranges from 50% to more than 95% in trabecular bone, e.g. (Turner et al., 1990),  $f_{vas} = 2 \dots 5\%$  in healthy cortical bone under normal physiological conditions, and reaches up to 50% in cortical bone under abnormal physiological

conditions, such as overtraining, drug treatment, or extreme age (McCarthy et al., 1990; Lees et al., 1994a; Sietsema, 1995). In contrast to  $f_{vas}$ ,  $\tilde{f}_{lac}$  depends only on the way osteoblasts work: when laying down osteoid, a typical fraction of osteoblasts become buried in this newly formed ultrastructure, leading to the formation of lacunae. Hence,  $\tilde{f}_{lac}$ , as opposed to  $f_{vas}$ , always lies within a quite narrow range of values.

Evaluation of the image shown in Fig. 1 of Lees et al. (1979a) [see Fig. 1(c)] through Eq. (15) renders  $f_{vas} = 3\%$ , typical for mammalian cortical bone under normal physiological conditions (Sietsema, 1995), considered in

Table 2  
Compilation of experimental data

| Tissue          | State | $\rho_{\mu, wet}$ or $\rho_{\mu, dry}$<br>(g/cm <sup>3</sup> )<br>given | $WF_{HA}^{\mu}$<br>(–)<br>given | $WF_{org}^{\mu}$<br>(–)<br>given | $f_{vas}$<br>(–)<br>given | $v_l$<br>(km/s)<br>given | $C_{ultra, 1111}^{exp}$<br>(GPa)<br>Eqs. (17) <sup>a</sup> ,<br>(18), (20),<br>(21), (42) | $\tilde{f}_{col}$<br>(–)<br>Eqs. (17) <sup>a</sup> , (18),<br>(20)–(22), (24),<br>(26), (28) | $\tilde{f}_{HA}$<br>(–)<br>Eqs. (17) <sup>a</sup> , (18),<br>(20)–(22), (23),<br>(25), (27) | $d_s$<br>(nm)<br>Eqs. (17) <sup>a</sup> ,<br>(18), (20),<br>(21), (36) |
|-----------------|-------|---|---------------------------------|----------------------------------|---------------------------|--------------------------|---|--|---|--|
| Cow tibia       | Wet   | 2.02 <sup>b</sup>   | 0.68 <sup>b</sup>               | 0.22 <sup>b</sup>                | 0.03 <sup>c</sup>         | 3.18 <sup>b</sup>        | 21.0  | 0.30   | 0.48  | 1.24   |
| Cow tibia       | Wet   | 1.99 <sup>b</sup>   | 0.66 <sup>b</sup>               | 0.22 <sup>b</sup>                | 0.03 <sup>c</sup>         | 3.18 <sup>b</sup>        | 20.7  | 0.29   | 0.46  | 1.25   |
| Cow tibia       | Wet   | 1.95 <sup>b</sup>   | 0.64 <sup>b</sup>               | 0.23 <sup>b</sup>                | 0.03 <sup>c</sup>         | 3.18 <sup>b</sup>        | 20.2  | 0.30   | 0.44  | 1.26   |
| Cow tibia       | Wet   | 2.01 <sup>b</sup>   | 0.66 <sup>b</sup>               | 0.22 <sup>b</sup>                | 0.03 <sup>c</sup>         | 3.16 <sup>b</sup>        | 20.6  | 0.29   | 0.46  | 1.25   |
| Cow tibia       | Wet   | 2.04 <sup>b</sup>   | 0.64 <sup>b</sup>               | 0.24 <sup>b</sup>                | 0.03 <sup>c</sup>         | 3.27 <sup>b</sup>        | 22.4  | 0.33   | 0.46  | 1.24   |
| Cow tibia       | Wet   | 2.05 <sup>b</sup>   | 0.67 <sup>b</sup>               | 0.21 <sup>b</sup>                | 0.03 <sup>c</sup>         | 3.26 <sup>b</sup>        | 22.4  | 0.29   | 0.48  | 1.24   |
| Cow tibia       | Wet   | 2.07 <sup>d</sup>   | 0.66 <sup>c</sup>               | 0.22 <sup>c</sup>                | 0.03 <sup>c</sup>         | 3.32 <sup>d</sup>        | 23.4  | 0.30   | 0.48  | 1.23   |
| Elephant radius | Wet   | 1.94 <sup>d</sup>   | 0.63 <sup>c</sup>               | 0.23 <sup>c</sup>                | 0.03 <sup>c</sup>         | 3.05 <sup>d</sup>        | 18.5  | 0.30   | 0.43  | 1.26   |
| Human femur     | Wet   | 1.93 <sup>d</sup>   | 0.70 <sup>e</sup>               | 0.23 <sup>c</sup>                | 0.03 <sup>c</sup>         | 3.13 <sup>d</sup>        | 19.4  | 0.30   | 0.47  | 1.26   |
| Deer antler     | Wet   | 1.78 <sup>d</sup>   | 0.51 <sup>e</sup>               | 0.31 <sup>c</sup>                | 0.03 <sup>c</sup>         | 2.38 <sup>d</sup>        | 10.3  | 0.37   | 0.32  | 1.29   |
| Deer antler     | Wet   | 1.74 <sup>d</sup>   | 0.52 <sup>e</sup>               | 0.32 <sup>c</sup>                | 0.03 <sup>c</sup>         | 2.40 <sup>d</sup>        | 10.2  | 0.37   | 0.32  | 1.30   |
| Cow tibia       | Dry   | 2.09 <sup>d</sup>   | 0.75 <sup>e</sup>               | 0.25 <sup>c</sup>                | 0.03 <sup>c</sup>         | 3.49 <sup>d</sup>        | 26.8  | 0.35   | 0.55  | 1.17   |
| Elephant radius | Dry   | 1.97 <sup>d</sup>   | 0.73 <sup>e</sup>               | 0.27 <sup>c</sup>                | 0.03 <sup>c</sup>         | 3.35 <sup>d</sup>        | 23.3  | 0.35   | 0.51  | 1.15   |
| Human femur     | Dry   | 1.92 <sup>d</sup>   | 0.75 <sup>e</sup>               | 0.25 <sup>c</sup>                | 0.03 <sup>c</sup>         | 3.33 <sup>d</sup>        | 22.4  | 0.32   | 0.51  | 1.14   |
| Deer antler     | Dry   | 1.76 <sup>d</sup>   | 0.62 <sup>e</sup>               | 0.38 <sup>e</sup>                | 0.03 <sup>c</sup>         | 2.81 <sup>d</sup>        | 14.6  | 0.45   | 0.38  | 1.10   |
| Deer antler     | Dry   | 1.82 <sup>d</sup>   | 0.62 <sup>e</sup>               | 0.38 <sup>e</sup>                | 0.03 <sup>c</sup>         | 2.91 <sup>d</sup>        | 16.2  | 0.47   | 0.40  | 1.11   |
| Rabbit femur    |       |   |                                 |                                  |                           |                          |   |  |   |  |
| BAPN-treated    | Wet   | 2.05 <sup>f</sup>   | 0.66 <sup>f</sup>               | 0.20 <sup>f</sup>                | 0.10 <sup>g</sup>         | 3.33 <sup>f</sup>        | 24.3  | 0.29   | 0.49  | 1.22   |
| BAPN-treated    | Wet   | 2.04 <sup>f</sup>   | 0.66 <sup>f</sup>               | 0.21 <sup>f</sup>                | 0.09 <sup>g</sup>         | 3.27 <sup>f</sup>        | 23.2  | 0.30   | 0.49  | 1.22   |
| BAPN-treated    | Wet   | 2.04 <sup>f</sup>   | 0.66 <sup>f</sup>               | 0.21 <sup>f</sup>                | 0.03 <sup>g</sup>         | 3.26 <sup>f</sup>        | 22.3  | 0.29   | 0.47  | 1.24   |
| BAPN-treated    | Wet   | 2.05 <sup>f</sup>   | 0.65 <sup>f</sup>               | 0.21 <sup>f</sup>                | 0.06 <sup>g</sup>         | 3.24 <sup>f</sup>        | 22.5  | 0.29   | 0.48  | 1.23   |
| BAPN-treated    | Wet   | 1.98 <sup>f</sup>   | 0.63 <sup>f</sup>               | 0.21 <sup>f</sup>                | 0.06 <sup>g</sup>         | 3.11 <sup>f</sup>        | 20.0  | 0.28   | 0.44  | 1.25   |
| BAPN-treated    | Wet   | 1.96 <sup>f</sup>   | 0.62 <sup>f</sup>               | 0.21 <sup>f</sup>                | 0.22 <sup>g</sup>         | 3.03 <sup>f</sup>        | 20.7  | 0.31   | 0.48  | 1.21   |
| Fluor-treated   | Wet   | 2.00 <sup>f</sup>   | 0.70 <sup>f</sup>               | 0.17 <sup>f</sup>                | 0.03 <sup>h</sup>         | 3.20 <sup>f</sup>        | 21.0  | 0.23   | 0.49  | 1.25   |
| Fluor-treated   | Wet   | 2.04 <sup>f</sup>   | 0.71 <sup>f</sup>               | 0.16 <sup>f</sup>                | 0.08 <sup>h</sup>         | 3.22 <sup>f</sup>        | 22.3  | 0.23   | 0.52  | 1.23   |
| Fluor-treated   | Wet   | 1.86 <sup>f</sup>   | 0.65 <sup>f</sup>               | 0.17 <sup>f</sup>                | 0.10 <sup>h</sup>         | 2.74 <sup>f</sup>        | 14.8  | 0.22   | 0.44  | 1.26   |
| Fluor-treated   | Wet   | 1.65 <sup>f</sup>   | 0.56 <sup>f</sup>               | 0.16 <sup>f</sup>                | 0.35 <sup>h</sup>         | 2.57 <sup>f</sup>        | 13.3  | 0.21   | 0.39  | 1.25   |

Experimental data for the microstructural wet and dry tissue mass densities,  $\rho_{\mu, wet}$  and  $\rho_{\mu, dry}$ , for the weight fractions of hydroxyapatite and organic matter,  $WF_{HA}^{\mu}$  and  $WF_{org}^{\mu}$ , for the volume fraction of Haversian canals,  $f_{vas}$ , and for the longitudinal sonic velocity in radial direction,  $v_l$ , of various mammalian bone specimens; evaluation of experimental data for determination of the ultrastructural normal stiffness component in radial direction,  $C_{ultra, 1111}^{exp}$ , of ultrastructural volume fractions of hydroxyapatite and collagen,  $\tilde{f}_{HA}$  and  $\tilde{f}_{col}$ , as well as of the neutron diffraction spacing  $d_s$ .

<sup>a</sup>Computed with  $\tilde{f}_{lac} = 2.1\%$ , according to Eq. (17) with  $f_{vas} = 3\%$  and  $f_{lac} = 2\%$ , determined from micrograph of Fig. 1 in (Lees et al., 1979a), see also Fig. 1(c), on the basis of Eqs. (15) and (16).

<sup>b</sup>Experimental data: Lees et al. (1979b).

<sup>c</sup>Determined from micrograph of Fig. 1 in (Lees et al., 1979a), see also Fig. 1(c), on the basis of Eq. (15).

<sup>d</sup>Experimental data: Lees et al. (1983).

<sup>e</sup>Experimental data: Lees (1987).

<sup>f</sup>Experimental data: Lees et al. (1994a).

<sup>g</sup>Determined from micrographs of Fig. 9 in (Lees et al., 1994a).

<sup>h</sup>Determined from micrographs of Fig. 10 in (Lees et al., 1994a).



the upper half of Table 2 and in Table 4. From the same picture, Eqs. (16) and (17) render  $f_{lac} = 2\%$  and  $\tilde{f}_{lac} = 2.1\%$ , the latter being typical for any kind of mammalian bone (Frost, 1962; Baylink and Wergedal, 1971; Morris et al., 1982; Zhang et al., 1998; Cowin, 1999). As regards the drug-treated rabbits investigated by Lees et al. (1994b), we determined  $f_{vas}$  as the volume fraction of Haversian canals from micrographs of diaphyseal cross sections of femoral specimens (Fig. 9 and 10 of Lees et al., 1994a, see column 6 of Table 2).

One may sum up  $f_{vas}$  and  $f_{lac}$  to get the total porosity discernable in a light microscope, which one may term microporosity  $f_{\mu por}$ ,

$$f_{\mu por} = f_{vas} + f_{lac}. \quad (18)$$

McCarthy et al. (1990) determined this microporosity from microradiographs of overtrained race horses, viewed under a low power microscope. Respective data are given in Table 6.  $\tilde{f}_{lac} = 2.1\%$  [Eq. (17) and discussion below] allows for determination of the (microstructural) volume fraction of the Haversian canals through

$$f_{vas} = \frac{f_{\mu por} - \tilde{f}_{lac}}{1 - \tilde{f}_{lac}} \quad (19)$$

see Table 6.

Determination of the ultrastructural volume fractions of mineral and collagen,  $\tilde{f}_{HA}$  and  $\tilde{f}_{col}$ , rests on volume measurements and weighing experiments on wet, dehydrated and demineralized cortical bone specimens, performed by Lees et al. (1979b, 1983); Lees (1987). These experiments give access to the microstructural weight fractions of water, of organic matter, and of mineral,  $WF_{H_2O}^\mu$ ,  $WF_{org}^\mu$  and  $WF_{HA}^\mu$ ; and to the microstructural mass densities of wet tissues,  $\rho_{\mu, wet}$  (with wet ultrastructure and water-filled lacunae and Haversian canals), and of dry tissues,  $\rho_{\mu, dry}$  (Tables 2 and 4). Combination of the latter values with microporosity  $f_{\mu por}$  [Eq. (18)] and the mass density of water,  $\rho_{H_2O} = 1 \text{ g/ml}$ , yields the mass density of (wet or dry) ultrastructure, see e.g. (Hellmich et al., 2004b),

$$\rho_{ultra, wet} = \frac{\rho_{\mu, wet} - \rho_{H_2O} f_{\mu por}}{1 - f_{\mu por}} \quad (20)$$

and

$$\rho_{ultra, dry} = \frac{\rho_{\mu, dry}}{1 - f_{\mu por}} \quad (21)$$

as well as the weight fraction of water-filled micropores in (wet) bone specimens, see e.g. (Torabian, 2004),

$$WF_{\mu por}^\mu = \frac{\rho_{H_2O} \times f_{\mu por}}{\rho_{\mu, wet}}, \quad (22)$$

where  $WF_{\mu por}^\mu$  allows for scale transition of the weight fractions from the microstructural to the ultrastructural scale, see e.g. (Torabian, 2004),

$$WF_{HA}^{ultra} = \frac{WF_{HA}^\mu}{1 - WF_{\mu por}^\mu}, \quad (23)$$

$$WF_{org}^{ultra} = \frac{WF_{org}^\mu}{1 - WF_{\mu por}^\mu}. \quad (24)$$

This completes the set of quantities necessary for computation of  $\tilde{f}_{HA}$  and  $\tilde{f}_{col}$  in wet tissues, through

$$\tilde{f}_{HA, wet} = \frac{\rho_{ultra, wet}}{\rho_{HA}} \times WF_{HA}^{ultra}, \quad (25)$$

$$\tilde{f}_{col, wet} = \frac{\rho_{ultra, wet}}{\rho_{col}} \times 0.9 \times WF_{org}^{ultra}, \quad (26)$$

where  $\rho_{HA} = 3.00 \text{ g/cm}^3$  (Lees, 1987; Hellmich, 2005) is the mass density of hydroxyapatite, and  $\rho_{col} \approx \rho_{org} = 1.41 \text{ g/cm}^3$  (Katz and Li, 1973; Lees, 1987) is the mass density of collagen. Eq. (26) accounts for the fact that, in mineralized tissues, about 90% per mass of the organic matter is collagen (Urist et al., 1983; Lees, 1987; Weiner and Wagner, 1998). For dry tissues,  $\tilde{f}_{HA}$  and  $\tilde{f}_{col}$  read as

$$\tilde{f}_{HA, dry} = \frac{WF_{HA}^{ultra}}{WF_{HA}^{ultra} + WF_{org}^{ultra}} \times \frac{\rho_{ultra, dry}}{\rho_{HA}}, \quad (27)$$

$$\tilde{f}_{col, dry} = \frac{0.9 WF_{org}^{ultra}}{WF_{HA}^{ultra} + WF_{org}^{ultra}} \times \frac{\rho_{ultra, dry}}{\rho_{col}} \quad (28)$$

see Tables 2 and 4 for a compilation of values determined from experiments of Lees et al. (1979b, 1983); Lees (1987); Lees et al. (1994a).

It is interesting to note that the dehydration–demineralization tests of Lees et al. (1979b); Lees (1987); Lees et al. (1995) reveal seemingly universal composition laws, valid throughout the entire vertebrate kingdom. In fact, the ultrastructural mineral volume fraction  $\tilde{f}_{HA}$  is linearly dependent on the ultrastructural mass density  $\rho_{ultra, wet}$ , which can be expressed by a regression function of the form (Hellmich and Ulm, 2002a; Hellmich, 2005)

$$\mathcal{F}_{\tilde{f}_{HA, wet}} = \mathcal{A} \times \rho_{ultra, wet} + \mathcal{B} \quad (29)$$

with  $\mathcal{A} = 0.59 \text{ ml/g}$  and  $\mathcal{B} = -0.75$ . Thereby, we considered a microporosity  $f_{\mu por} = 5\%$  according to Fig. 1(c) for the long bone tissues of Lees et al. (1979b); Lees (1987) and  $f_{\mu por} = 0\%$  for the hyperpneumatic tissues of Lees (1987); Lees et al. (1995), see Fig. 4. The statistical relevance of this relationship  $\mathcal{F}_{\tilde{f}_{HA, wet}}(\rho_{ultra, wet})$  is underlined by a correlation coefficient of  $r^2 = 97\%$ .

Combination of (29) with

$$\rho_{ultra, wet} = \tilde{f}_{H_2O, wet} \rho_{H_2O} + \tilde{f}_{org, wet} \rho_{org} + \tilde{f}_{HA, wet} \rho_{HA} \quad (30)$$

with  $1 = \tilde{f}_{org} + \tilde{f}_{H_2O} + \tilde{f}_{HA}$ , and with  $\tilde{f}_{col} = 0.9 \times \tilde{f}_{org}$  [compare (26)] yields a function for the collagen content in wet tissues (Torabian, 2004; Hellmich, 2005)

$$\mathcal{F}_{\tilde{f}_{col, wet}}(\rho_{ultra, wet}) = 0.9 \times \mathcal{F}_{\tilde{f}_{org, wet}}(\rho_{ultra, wet}),$$

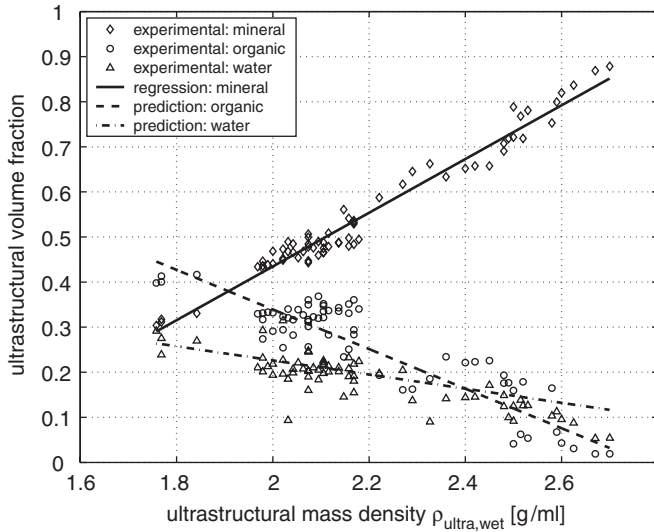


Fig. 4. Composition of bone ultrastructure; linear relationship between ultrastructural mineral volume fraction and tissue mass density (see diamond-marked experimental data of Lees et al., 1979b; Lees, 1987; Lees et al., 1995, and solid-line regression function Eq. (29)); Predictions of ultrastructural organic and water volume fraction (dashed and dash-dotted lines representing Eqs. (31) and (32)) agree well with circle-marked and triangle-marked experimental data of Lees et al. (1979b); Lees (1987); Lees et al. (1995); see also (Torabia, 2004; Hellmich, 2005).

whereby

$$\mathcal{F}_{\tilde{f}_{org,wet}}(\rho_{ultra,wet}) = \frac{1}{\rho_{H_2O} - \rho_{org}} \{ \mathcal{F}_{\tilde{f}_{HA,wet}}(\rho_{ultra,wet}) \times [\rho_{HA} - \rho_{H_2O}] - \rho_{ultra,wet} + \rho_{H_2O} \}. \quad (31)$$

This prediction  $\mathcal{F}_{\tilde{f}_{org,wet}}(\rho_{ultra,wet})$  (dashed line in Fig. 4) compares well with the experimental data of Lees et al. (1979b); Lees (1987); Lees et al. (1995), indicated by circles in Fig. 4. The same is true for the ultrastructural water volume fraction,

$$\mathcal{F}_{\tilde{f}_{H_2O,wet}}(\rho_{ultra,wet}) = 1 - \mathcal{F}_{\tilde{f}_{org,wet}}(\rho_{ultra,wet}) - \mathcal{F}_{\tilde{f}_{HA,wet}}(\rho_{ultra,wet}) \quad (32)$$

see dash-dotted line and triangle markers in Fig. 4. The relationships shown in Fig. 4 provoke the seemingly reasonable concept of a constant ratio between mineral increase and water/collagen decrease during biomineralization. Although the experiments of Lees et al. (1979b); Lees (1987); Lees et al. (1995) were all performed on cortical bone, the strong similarity of the ultrastructure in cortical bone and of that in trabecular bone (Gong et al., 1964) renders the relationships of Fig. 4 very probable to be valid also for trabecular bone.

The ‘stoichiometric’ functions (29), (31), and (32) are useful to estimate the ultrastructural composition of the bone specimens documented by McCarthy et al. (1990), see Table 6. In detail, the microstructural (= apparent = macroscopic) mass densities of specimens with empty Haversian canals,  $\rho_{\mu,empty}$ , and corresponding microporos-

ities  $f_{\mu,por}$  give access, via  $\tilde{f}_{lac} = 2.1\%$  and  $f_{vas}$  according to (19), to the mass density of the extravascular bone material (with water-filled lacunae),

$$\rho_{exvas} = \frac{\rho_{\mu,empty}}{1 - f_{vas}} \quad (33)$$

and to the density of the extracellular bone matrix or ultrastructure, reading as

$$\rho_{ultra,wet} = \frac{\rho_{exvas} - \rho_{H_2O} \tilde{f}_{lac}}{1 - \tilde{f}_{lac}}. \quad (34)$$

Use of  $\rho_{ultra,wet}$  in (29) and (31) yields the ultrastructural composition values  $\tilde{f}_{HA}$  and  $\tilde{f}_{col}$  (Table 6, columns 8 and 9).

The ultrastructural volume fraction of the fibrils and the extrafibrillar space,  $\tilde{f}_{fib}$  and  $\tilde{f}_{ef}$ , [Fig. 3(d)] can be quantified on the basis of the generalized packing model of Lees et al. (1984b); Lees (1987), through

$$\tilde{f}_{fib} = \tilde{f}_{col} \times \frac{v_{fib}}{v_{col}}, \quad v_{fib} = b d_s 5D, \quad (35)$$

where  $\tilde{f}_{col}$  (wet or dry) is determined according to Eq. (26), (28), or (31), respectively.  $v_{col} = 335.6 \text{ nm}^3$  is the volume of a single collagen molecule (Lees, 1987).  $v_{fib}$  is the volume of one rhomboidal fibrillar unit with length  $5D$ , width  $b$ , and height  $d_s$ .  $b = 1.47 \text{ nm}$  is an average (rigid) collagen crosslink length valid for all mineralized tissues (Lees et al., 1984b),  $D \approx 64 \text{ nm}$  is the axial macroperiod of staggered assemblies of type I collagen, and  $d_s$  is the tissue-specific neutron diffraction spacing between collagen molecules, which depends on the mineralization and the hydration state of the tissue (Lees et al., 1984a; Bonar et al., 1985; Lees et al., 1994b). For wet tissues,  $d_s$  can be given in a dimensionless form (Hellmich and Ulm, 2003), as a function of  $\rho_{ultra,wet}$  only. For the rather narrow range of tissue mass densities considered here, this function can be linearly approximated through

$$d_s = \mathcal{C} \times \rho_{ultra} + \mathcal{D}, \quad (36)$$

where  $\mathcal{C} = -0.2000 \text{ nm}/(\text{g cm}^{-3})$ ,  $\mathcal{D} = 1.6580 \text{ nm}$  for wet tissues; and  $\mathcal{C} = 0.1923 \text{ nm}/(\text{g cm}^{-3})$ ,  $\mathcal{D} = 0.7465 \text{ nm}$  for dry tissues (Lees et al., 1984a; Lees, 1987). Values for  $d_s$  and  $\tilde{f}_{fib}$ , derived from experiments of Lees et al. (1979b); Lees et al. (1983); Lees (1987); Lees et al. (1994a); McCarthy et al. (1990); Ashman and Rho (1988), are compiled in 3, 5, 7, and 8.

The volume fractions for scales below the ultrastructure can be derived directly from  $\tilde{f}_{fib}$  and  $\tilde{f}_{col}$ , on the basis of the finding of Hellmich and Ulm (2001, 2003) that the average hydroxyapatite concentration in the extra-collagenous space of the ultrastructure of wet mineralized tissues is the same inside and outside the fibrils. Accordingly, the relative amount of hydroxyapatite in the extrafibrillar space reads as (Hellmich and Ulm, 2001, 2003)

$$\phi_{HA,ef} = \frac{1 - \tilde{f}_{fib,wet}}{1 - \tilde{f}_{col,wet}}. \quad (37)$$

Table 3  
Compilation of experimental data

| Tissue          | State | $\tilde{f}_{col}$<br>(–)<br>Table 2 | $\tilde{f}_{HA}$<br>(–)<br>Table 2 | $d_s$<br>(nm)<br>Table 2 | $\tilde{f}_{fib}$<br>(–)<br>Eq. (35) | $\check{f}_{HA}$<br>(–)<br>Eqs. (37),<br>(39) | $\check{f}_{HA}$<br>(–)<br>Eqs. (37),<br>(38) | $\check{f}_{col}$<br>(–)<br>Eqs. (40),<br>(41) |
|-----------------|-------|-------------------------------------|------------------------------------|--------------------------|--------------------------------------|---|---|--|
| Cow tibia       | Wet   | 0.30                                | 0.48                               | 1.24                     | 0.52                                 | 0.68  | 0.29  | 0.42   |
| Cow tibia       | Wet   | 0.29                                | 0.46                               | 1.25                     | 0.51                                 | 0.65  | 0.28  | 0.41   |
| Cow tibia       | Wet   | 0.30                                | 0.44                               | 1.26                     | 0.53                                 | 0.62  | 0.27  | 0.41   |
| Cow tibia       | Wet   | 0.29                                | 0.46                               | 1.25                     | 0.51                                 | 0.66  | 0.28  | 0.41   |
| Cow tibia       | Wet   | 0.33                                | 0.46                               | 1.24                     | 0.58                                 | 0.68  | 0.29  | 0.47   |
| Cow tibia       | Wet   | 0.29                                | 0.48                               | 1.24                     | 0.50                                 | 0.68  | 0.29  | 0.41   |
| Cow tibia       | Wet   | 0.30                                | 0.48                               | 1.23                     | 0.53                                 | 0.69  | 0.29  | 0.43   |
| Elephant radius | Wet   | 0.30                                | 0.43                               | 1.26                     | 0.53                                 | 0.61  | 0.27  | 0.41   |
| Human femur     | Wet   | 0.30                                | 0.47                               | 1.26                     | 0.53                                 | 0.68  | 0.29  | 0.42   |
| Deer antler     | Wet   | 0.37                                | 0.32                               | 1.29                     | 0.67                                 | 0.51  | 0.23  | 0.48   |
| Deer antler     | Wet   | 0.37                                | 0.32                               | 1.30                     | 0.68                                 | 0.51  | 0.23  | 0.49   |
| Cow tibia       | Dry   | 0.35                                | 0.55                               | 1.17                     | 0.57                                 | 0.85  | 0.33  | 0.52   |
| Elephant radius | Dry   | 0.35                                | 0.51                               | 1.15                     | 0.57                                 | 0.78  | 0.30  | 0.50   |
| Human femur     | Dry   | 0.32                                | 0.51                               | 1.14                     | 0.51                                 | 0.74  | 0.28  | 0.44   |
| Deer antler     | Dry   | 0.45                                | 0.38                               | 1.10                     | 0.69                                 | 0.69  | 0.25  | 0.59   |
| Deer antler     | Dry   | 0.47                                | 0.40                               | 1.11                     | 0.73                                 | 0.74  | 0.27  | 0.64   |
| Rabbit femur    |       |                                     |                                    |                          |                                      |   |   |  |
| BAPN-treated    | Wet   | 0.29                                | 0.49                               | 1.22                     | 0.49                                 | 0.69  | 0.29  | 0.40   |
| BAPN-treated    | Wet   | 0.30                                | 0.49                               | 1.22                     | 0.51                                 | 0.70  | 0.29  | 0.42   |
| BAPN-treated    | Wet   | 0.29                                | 0.47                               | 1.24                     | 0.50                                 | 0.66  | 0.28  | 0.40   |
| BAPN-treated    | Wet   | 0.29                                | 0.48                               | 1.23                     | 0.51                                 | 0.67  | 0.28  | 0.41   |
| BAPN-treated    | Wet   | 0.28                                | 0.44                               | 1.25                     | 0.50                                 | 0.62  | 0.27  | 0.39   |
| BAPN-treated    | Wet   | 0.31                                | 0.48                               | 1.21                     | 0.53                                 | 0.69  | 0.28  | 0.43   |
| Fluor-treated   | Wet   | 0.23                                | 0.49                               | 1.25                     | 0.40                                 | 0.64  | 0.27  | 0.31   |
| Fluor-treated   | Wet   | 0.23                                | 0.52                               | 1.23                     | 0.39                                 | 0.67  | 0.28  | 0.31   |
| Fluor-treated   | Wet   | 0.22                                | 0.44                               | 1.26                     | 0.39                                 | 0.56  | 0.25  | 0.29   |
| Fluor-treated   | Wet   | 0.21                                | 0.39                               | 1.25                     | 0.37                                 | 0.49  | 0.21  | 0.27   |

Experimental data for ultrastructural volume fractions of hydroxyapatite and collagen,  $\tilde{f}_{HA}$  and  $\tilde{f}_{col}$ , and for the neutron diffraction spacing  $d_s$ , of various mammalian bone specimens, taken from Table 2; evaluation of experimental data for determination of ultrastructural volume fractions of fibrils,  $\tilde{f}_{fib}$ , of extrafibrillar and fibrillar volume fraction of mineral,  $\check{f}_{HA}$  and  $\check{f}_{HA}$ , and of (molecular) collagen volume fraction within the wet collagen matrix,  $\check{f}_{col}$ .

With this value at hand, the mineral volume fractions in the fibrillar [Fig. 3(b)] and the extrafibrillar space [Fig. 3(c)] are, for both wet and dry tissues,

$$\check{f}_{HA} = \frac{\tilde{f}_{HA}(1 - \phi_{HA,ef})}{\tilde{f}_{fib}}, \quad (38)$$

$$\check{f}_{HA} = \frac{\phi_{HA,ef}\tilde{f}_{HA}}{\tilde{f}_{ef}} \quad (39)$$

see Tables 3 and 5 for the mammalian bones tested by Lees et al. (1979b, 1983); Lees (1987); Lees et al. (1994a), Table 7 for the equine bones tested by McCarthy et al. (1990), and Table 8 for the human and bovine bones tested by Ashman and Rho (1988).

Within the fibril, comprising the phases hydroxyapatite and wet collagen, the volume fraction of the latter reads as

$$\check{f}_{wetcol} = 1 - \check{f}_{HA}. \quad (40)$$

Finally, the volume fraction of (molecular) collagen at the wet collagen level [Fig. 3(a)] can be calculated from  $\check{f}_{col}$

(wet or dry), through

$$\check{f}_{col} = \frac{\tilde{f}_{col}}{\tilde{f}_{wetcol}} \quad (41)$$

see Tables 3 and 5 for the mammalian bones tested by Lees et al. (1979b, 1983); Lees (1987); Lees et al. (1994a), Table 7 for the equine bones tested by McCarthy et al. (1990), and Table 8 for the human and bovine bones tested by Ashman and Rho (1988).

#### 4.4. Elasticity experiments on bone—experimental set IIb

Ultrasonic experiments are based on the measurements of velocities of plane waves. If the waves travel along the principal material directions of an orthotropic material, through a 3D medium, the wave propagation velocities allow for determination of the material stiffness constants, according to the theory of elastic waves (Fedorov, 1968)

$$C_{1111} = \rho v_1^2, \quad (42)$$

$$C_{2222} = \rho v_2^2, \quad (43)$$

$$C_{3333} = \rho v_3^2, \quad (44)$$

$$C_{2323} = G_{23} = \rho v_{23}^2, \quad (45)$$

$$C_{1313} = G_{13} = \rho v_{13}^2, \quad (46)$$

$$C_{1212} = G_{12} = \rho v_{12}^2, \quad (47)$$

$$C_{1122} = -\rho v_{12}^2 + \{(\rho v_1^2 + \rho v_{12}^2 - 2\rho \times v_{12/12}^2) \times (\rho v_2^2 + \rho v_{12}^2 - 2\rho \times v_{12/12}^2)\}^{1/2}, \quad (48)$$

$$C_{1133} = -\rho v_{13}^2 + \{(\rho v_1^2 + \rho v_{13}^2 - 2\rho \times v_{13/13}^2) \times (\rho v_3^2 + \rho v_{13}^2 - 2\rho \times v_{13/13}^2)\}^{1/2}, \quad (49)$$

$$C_{2233} = -\rho v_{23}^2 + \{(\rho v_2^2 + \rho v_{23}^2 - 2\rho \times v_{23/23}^2) \times (\rho v_3^2 + \rho v_{23}^2 - 2\rho \times v_{23/23}^2)\}^{1/2}. \quad (50)$$

Hereby,  $\rho$  refers to the mass density of the material (at the ultrastructural or extravascular scale, depending on the wave length),  $v_i$  refers to a longitudinal wave travelling in the  $i$ -direction, and  $v_{ij}$  denotes the velocity of transverse waves traveling in the  $i$ -direction with particle motion in the  $j$ -direction.  $v_{ij/ij}$  denotes the velocity of a (quasi-)longitudinal or a (quasi-)transverse wave traveling in the  $(i+j)/\sqrt{2}$ -direction with particle motion in the  $i-j$  plane. Indices 1 and 2 refer to the radial (transverse) direction, and 3 refers to the axial (longitudinal) direction.

A typical device for the transmission of an elastic wave through a bone sample can be sketched as follows: a transmitter excites a specimen surface by a short impulse (signal) (Yoon and Katz, 1976) or by a continuous wave (Ashman and Rho, 1988), with an excitation frequency  $f$ . After the transition time  $t$ , a receiver records the arrival of the signal at the opposite surface of the specimen. Specimen length  $l$  and transition time  $t$  allow for computation of propagation velocity  $v = l/t$ . Excitation frequency  $f$  and propagation velocity  $v$  govern the wave length  $\lambda$ , through

$$\lambda = \frac{v}{f}. \quad (51)$$

In terms of micromechanics (see Section 2), the wavelength  $\lambda$  (a measure for  $\mathcal{L}$ ) is significantly larger than the characteristic length of a representative volume element (RVE) of the experimentally characterized material. In this way, it is guaranteed that the RVE is loaded by (approximately) homogeneous strains (Fig. 5). This is consistent with the fact that the scanning acoustic microscope allows for a resolution which is finer than the wavelength, as explicitly stated on p. 905 of the 1975 Science paper of Lemons and Quate (1975), and as can easily be derived from data reported from numerous studies on bone, e.g. (Katz et al., 2001) ( $\lambda \approx 9 \mu\text{m} > 2.5 \mu\text{m}$  resolution) or (Eckardt and Hein, 2001) ( $\lambda \approx 3.8 \mu\text{m} > 2.5 \mu\text{m}$  resolution). Thus, rather than the wave length, the diffraction-limited minimum diameter (spot) of the focussed beam in the object plane governs the resolution (Lemons and Quate, 1974; Khuri-Yakub, 1993; Yu and Boseck, 1995). The scale separation between the wave length and the characteristic length of the material (RVE) allows for identification of the hierarchical levels whose elastic properties are ultrasonically ‘detected’ at different frequencies (Fig. 5):

- In the ultrasonic tests of Lees et al. (1979b, 1983, 1994a), excitation frequencies of 10 MHz were used. Given a typical wave propagation velocity of  $\sim 3 \text{ km/s}$  in bone specimens, the characteristic corresponding wave lengths  $\lambda = \mathcal{L}$  were of the order of  $300 \mu\text{m}$ . The characteristic length of the experimentally characterized material must obey  $\ell \ll 300 \mu\text{m}$ , which is the case for the ultrastructure with  $\ell = 5\text{--}10 \mu\text{m}$  [Figs. 1(e) and 3(d)]. Hence, the wave velocities measured in the 10 MHz—frequency regime refer to the *elastic stiffness of bone ultrastructure*.
- In the ultrasonic tests performed by Ashman et al. (1984); Ashman and Rho (1988); McCarthy et al. (1990), excitation frequencies of 2.25 MHz were used. Given a typical velocity of  $\sim 3 \text{ km/s}$  in these bone specimens, corresponding wavelengths were, according to Eq. (51), of the order of 1.3 mm. The characteristic length  $\ell$  of experimentally characterized material must be significantly smaller than 1.3 mm. This is the case for the extravascular bone material with  $\ell \approx 100 \mu\text{m}$ , see

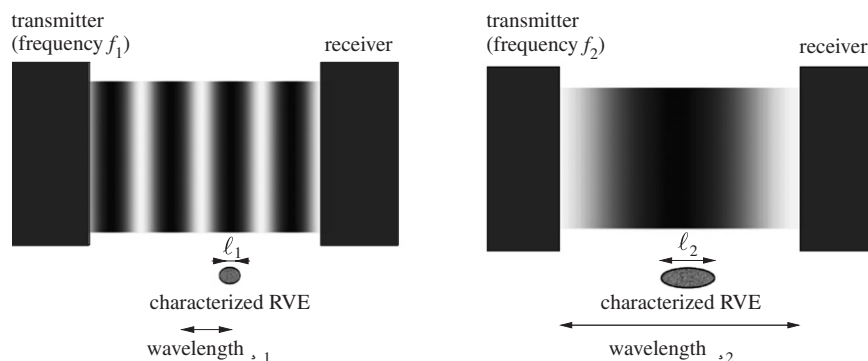


Fig. 5. Schematic, grey-scale based illustration of stress magnitude in specimens tested ultrasonically with different frequencies ( $f_1 > f_2$ ): characterization of material elements (RVEs) with characteristic lengths  $\ell$  separated by scale from the wavelength  $\lambda$ .



Fig. 3(e). Hence, the wave velocities measured in the 2.25 MHz—frequency regime refer to the stiffness of extravascular bone material.

#### 4.4.1. Ultrasonic tests with 10 MHz frequency—characterization of ultrastructure

Lees et al. (1979b, 1983, 1994a) reported velocities  $v_1$  and  $v_3$  of longitudinal waves traveling in the radial and in the axial direction of cortical bone specimens; along with microstructural mass densities of wet specimens,  $\rho_{\mu, \text{wet}}$ , and vascular porosity  $f_{\text{vas}}$  (Tables 2 and 4, columns 3, 6 and 7). The latter give access to ultrastructural mass densities  $\rho_{\text{ultra, wet}}$  and  $\rho_{\text{ultra, dry}}$  via Eq. (17) with  $\tilde{f}_{\text{lac}} = 2.1\%$ , Eqs. (18), (20), and (21). Insertion of these values for  $v_1$ ,  $v_3$ , and  $\rho = \rho_{\text{ultra, wet}}$  or  $\rho = \rho_{\text{ultra, dry}}$ , into Eqs. (42) and (44) yields specimen-specific experimental stiffness values  $C_{\text{ultra, 1111}}^{\text{exp}}$  and  $C_{\text{ultra, 3333}}^{\text{exp}}$ , see Tables 2 and 4, column 8, as well as Fig. 6 (x-axis).

#### 4.4.2. Ultrasonic tests with 2.25 MHz frequency—characterization of extravascular bone material

McCarthy et al. (1990) reported velocities of longitudinal waves traveling in the radial (transverse) direction of specimens from the dorsal cortex of equine third metacarpus,

$v_1 \approx v_2$ , and velocities of longitudinal waves traveling in the axial (longitudinal) direction of the aforementioned equine bone specimens,  $v_3$ ; along with microstructural (= apparent = macroscopic) mass densities of specimens with empty Haversian canals,  $\rho_{\mu, \text{empty}}$ , and microporosity  $f_{\mu\text{por}}$  (Table 6, columns 1–4). The latter give access to extravascular mass densities  $\rho_{\text{exvas}}$  via Eq. (19) with  $\tilde{f}_{\text{lac}} = 2.1\%$  and Eq. (33). Insertion of these values for  $v_1$ ,  $v_3$ , and  $\rho = \rho_{\text{exvas}}$  into Eqs. (42) and (44) yields specimen-specific experimental stiffness values  $C_{\text{exvas, 1111}}^{\text{exp}}$  and  $C_{\text{exvas, 3333}}^{\text{exp}}$ , see Table 6, columns 5 and 6, as well as Fig. 7 (x-axis).

Ashman and Rho (1988) reported velocities of longitudinal waves traveling in the axial (longitudinal) direction of bovine and human trabecular bone specimens,  $v_3$ ; along with extravascular mass densities  $\rho_{\text{exvas}}$  (Table 8, columns 3 and 4). Insertion of these values for  $v_3$  and  $\rho = \rho_{\text{exvas}}$  into Eq. (44) yields specimen-specific experimental stiffness values  $C_{\text{exvas, 3333}}^{\text{exp}}$ , see Table 8, column 5, and Fig. 7 (x-axis).

Also Ashman et al. (1984) used wave lengths referring to the extravascular bone material, but based computation of stiffness values according to Eq. (42)–(50) on a microstructural mass density  $\rho_{\mu, \text{wet}} = 1.90 \text{ g/ml}$ , averaged over 60 human femoral specimens. Hence, these stiffness values

Table 4  
Compilation of experimental data

| Tissue          | State | $\rho_{\mu, \text{wet}}$ or $\rho_{\mu, \text{dry}}$<br>(g/cm <sup>3</sup> )<br>given | $WF_{\text{HA}}^{\mu}$<br>(–)<br>given | $WF_{\text{org}}^{\mu}$<br>(–)<br>given | $f_{\text{vas}}$<br>(–)<br>given | $v_3$<br>(km/s)<br>given | $C_{\text{ultra, 3333}}^{\text{exp}}$<br>(GPa)<br>Eqs. (17) <sup>a</sup><br>(18), (20),<br>(21), (44) | $\tilde{f}_{\text{col}}$<br>(–)<br>Eqs. (17) <sup>a</sup> , (18),<br>(20)–(22), (24),<br>(26), (28) | $\tilde{f}_{\text{HA}}$<br>(–)<br>Eqs. (17) <sup>a</sup> , (18),<br>(20)–(22), (23),<br>(25), (27) | $d_s$<br>(nm)<br>Eqs. (17) <sup>a</sup><br>(18), (20),<br>(21), (36) |
|-----------------|-------|---|--|---|----------------------------------|--------------------------|---|---|--|--|
| Cow tibia       | Wet   | 2.06 <sup>b</sup>   | 0.66 <sup>b</sup>                      | 0.22 <sup>b</sup>                       | 0.03 <sup>c</sup>                | 3.92 <sup>b</sup>        | 32.5  | 0.30  | 0.48   | 1.23   |
| Cow tibia       | Wet   | 2.05 <sup>b</sup>   | 0.66 <sup>b</sup>                      | 0.22 <sup>b</sup>                       | 0.03 <sup>c</sup>                | 3.92 <sup>b</sup>        | 32.4  | 0.30  | 0.47   | 1.24   |
| Cow tibia       | Wet   | 2.02 <sup>b</sup>   | 0.62 <sup>b</sup>                      | 0.24 <sup>b</sup>                       | 0.03 <sup>c</sup>                | 3.81 <sup>b</sup>        | 30.1  | 0.32  | 0.44   | 1.24   |
| Cow tibia       | Wet   | 2.02 <sup>b</sup>   | 0.63 <sup>b</sup>                      | 0.23 <sup>b</sup>                       | 0.03 <sup>c</sup>                | 3.86 <sup>b</sup>        | 30.9  | 0.31  | 0.44   | 1.24   |
| Cow tibia       | Wet   | 2.00 <sup>b</sup>   | 0.64 <sup>b</sup>                      | 0.23 <sup>b</sup>                       | 0.03 <sup>c</sup>                | 3.90 <sup>b</sup>        | 31.2  | 0.31  | 0.45   | 1.25   |
| Cow tibia       | Wet   | 2.05 <sup>b</sup>   | 0.64 <sup>b</sup>                      | 0.23 <sup>b</sup>                       | 0.03 <sup>c</sup>                | 3.88 <sup>b</sup>        | 31.7  | 0.32  | 0.46   | 1.24   |
| Cow tibia       | Wet   | 2.10 <sup>b</sup>   | 0.67 <sup>b</sup>                      | 0.21 <sup>b</sup>                       | 0.03 <sup>c</sup>                | 3.88 <sup>b</sup>        | 32.5  | 0.30  | 0.49   | 1.23   |
| Cow tibia       | Wet   | 2.08 <sup>b</sup>   | 0.66 <sup>b</sup>                      | 0.22 <sup>b</sup>                       | 0.03 <sup>c</sup>                | 3.92 <sup>b</sup>        | 32.8  | 0.30  | 0.48   | 1.23   |
| Cow tibia       | Wet   | 2.06 <sup>d</sup>   | 0.66 <sup>c</sup>                      | 0.22 <sup>c</sup>                       | 0.03 <sup>c</sup>                | 4.18 <sup>d</sup>        | 37.0  | 0.30  | 0.48   | 1.23   |
| Elephant radius | Wet   | 1.93 <sup>d</sup>   | 0.63 <sup>c</sup>                      | 0.23 <sup>c</sup>                       | 0.03 <sup>c</sup>                | 3.89 <sup>d</sup>        | 29.9  | 0.30  | 0.43   | 1.26   |
| Human femur     | Wet   | 1.96 <sup>d</sup>   | 0.70 <sup>e</sup>                      | 0.23 <sup>c</sup>                       | 0.03 <sup>c</sup>                | 3.76 <sup>d</sup>        | 28.4  | 0.30  | 0.48   | 1.26   |
| Deer antler     | Wet   | 1.74 <sup>d</sup>   | 0.51 <sup>c</sup>                      | 0.31 <sup>c</sup>                       | 0.03 <sup>c</sup>                | 3.08 <sup>d</sup>        | 16.9  | 0.36  | 0.31   | 1.30   |
| Deer antler     | Wet   | 1.73 <sup>d</sup>   | 0.52 <sup>c</sup>                      | 0.32 <sup>c</sup>                       | 0.03 <sup>c</sup>                | 3.15 <sup>d</sup>        | 17.5  | 0.37  | 0.32   | 1.30   |
| Cow tibia       | Dry   | 2.10 <sup>d</sup>   | 0.75 <sup>c</sup>                      | 0.25 <sup>c</sup>                       | 0.03 <sup>c</sup>                | 4.47 <sup>d</sup>        | 44.2  | 0.35  | 0.55   | 1.17   |
| Elephant radius | Dry   | 1.97 <sup>d</sup>   | 0.73 <sup>c</sup>                      | 0.27 <sup>c</sup>                       | 0.03 <sup>c</sup>                | 4.22 <sup>d</sup>        | 36.9  | 0.35  | 0.51   | 1.15   |
| Human femur     | Dry   | 1.96 <sup>d</sup>   | 0.75 <sup>c</sup>                      | 0.25 <sup>c</sup>                       | 0.03 <sup>c</sup>                | 3.97 <sup>d</sup>        | 32.5  | 0.33  | 0.52   | 1.14   |
| Deer antler     | Dry   | 1.75 <sup>d</sup>   | 0.62 <sup>c</sup>                      | 0.38 <sup>c</sup>                       | 0.03 <sup>c</sup>                | 3.72 <sup>d</sup>        | 25.5  | 0.44  | 0.38   | 1.10   |
| Deer antler     | Dry   | 1.83 <sup>d</sup>   | 0.62 <sup>c</sup>                      | 0.38 <sup>c</sup>                       | 0.03 <sup>c</sup>                | 3.93 <sup>d</sup>        | 29.8  | 0.47  | 0.40   | 1.12   |

Experimental data for the microstructural wet and dry tissue mass densities,  $\rho_{\mu, \text{wet}}$  and  $\rho_{\mu, \text{dry}}$ , for the weight fractions of hydroxyapatite and organic matter,  $WF_{\text{HA}}^{\mu}$  and  $WF_{\text{org}}^{\mu}$ , for the volume fraction of Haversian canals,  $f_{\text{vas}}$ , and for the longitudinal sonic velocity in axial direction,  $v_3$ , of various mammalian bone specimens; evaluation of experimental data for determination of the ultrastructural normal stiffness component in axial direction,  $C_{\text{ultra, 3333}}^{\text{exp}}$ , of ultrastructural volume fractions of hydroxyapatite and collagen,  $\tilde{f}_{\text{HA}}$  and  $\tilde{f}_{\text{col}}$ , as well as of the neutron diffraction spacing  $d_s$ .

<sup>a</sup>Computed with  $\tilde{f}_{\text{lac}} = 2.1\%$ , according to Eq. (17) with  $f_{\text{vas}} = 3\%$  and  $f_{\text{lac}} = 2\%$ , determined from micrograph of Fig. 1 in (Lees et al., 1979a), see also Fig. 1(c), on the basis of Eqs. (15) and (16).

<sup>b</sup>Experimental data: (Lees et al., 1979b).

<sup>c</sup>Determined from micrograph of Fig. 1 in (Lees et al., 1979a), see also Fig. 1(c), on the basis of Eq. (15).

<sup>d</sup>Experimental data: (Lees et al., 1983).

<sup>e</sup>Experimental data: (Lees, 1987).

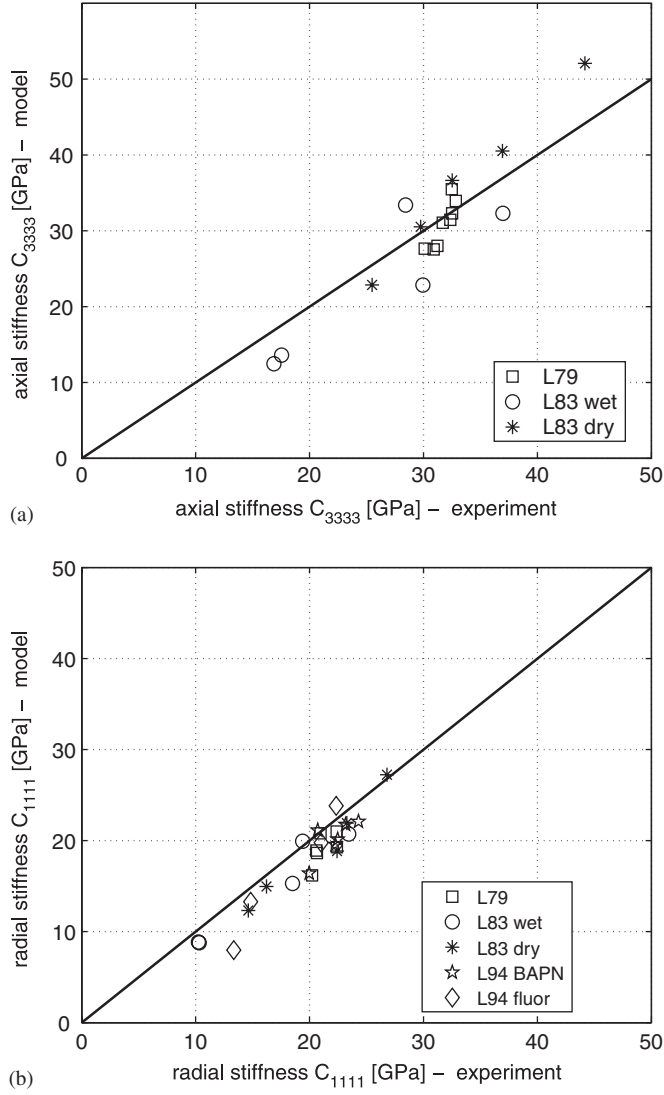


Fig. 6. Comparison between model predictions and experiments at the extracellular or ultrastructural scale [Fig. 3(d)]: (a) axial normal stiffness values, (b) radial normal stiffness values; (10 MHz ultrasonic experiments: L 79... (Lees et al., 1979b), L83... (Lees et al., 1983), L94... (Lees et al., 1994a)).

have to be corrected by the factor

$$\frac{\rho_{exvas}}{\rho_{\mu,wet}} = \frac{\rho_{\mu,wet} - \rho_{H_2O} f_{vas}}{(1 - f_{vas}) \rho_{\mu,wet}} \quad (52)$$

with  $f_{vas} = 3\%$  (Table 4, row 11, column 6), yielding the following experimental stiffness tensor:

$$\mathbb{C}_{exvas}^{exp} = \begin{pmatrix} C_{1111} & C_{1122} & C_{1133} & 0 & 0 & 0 \\ C_{1122} & C_{2222} & C_{2233} & 0 & 0 & 0 \\ C_{1133} & C_{2233} & C_{3333} & 0 & 0 & 0 \\ 0 & 0 & 0 & 2C_{2323} & 0 & 0 \\ 0 & 0 & 0 & 0 & 2C_{1313} & 0 \\ 0 & 0 & 0 & 0 & 0 & 2C_{1212} \end{pmatrix}$$

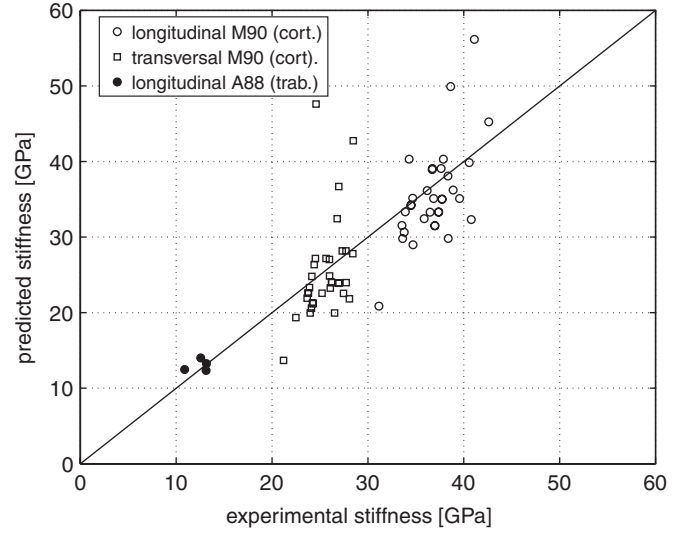


Fig. 7. Comparison between model predictions and experiments at the extravascular scale (2.25 MHz ultrasonic experiments of A88... (Ashman and Rho, 1988), M90... (McCarthy et al. (1990)).

$$= \begin{pmatrix} 18.5 & 10.3 & 10.4 & 0 & 0 & 0 \\ 10.3 & 20.8 & 11.0 & 0 & 0 & 0 \\ 10.4 & 11.0 & 28.4 & 0 & 0 & 0 \\ 0 & 0 & 0 & 12.9 & 0 & 0 \\ 0 & 0 & 0 & 0 & 11.5 & 0 \\ 0 & 0 & 0 & 0 & 0 & 9.3 \end{pmatrix}. \quad (53)$$

#### 4.5. Comparison between stiffness predictions and experiments

The stiffness values at the extracellular (ultrastructural) and extravascular scale predicted by the five-step homogenization scheme (Fig. 3) for tissue-specific volume fractions (Section 4.3, experimental set IIa) on the basis of tissue-independent ‘universal’ phase stiffness properties (experimental set I, Table 1) are compared to corresponding experimentally determined tissue-specific stiffness values from experimental set IIb (Section 4.4). To quantify the model’s predictive capabilities, we consider the mean and the standard deviation of the relative error between stiffness predictions and experiments,

$$\bar{e} = \frac{1}{n} \sum e_i = \frac{1}{n} \sum \frac{C_{ijkl}^{pred} - C_{ijkl}^{exp}}{C_{ijkl}^{exp}}, \quad (54)$$

$$e_s = \left[ \frac{1}{n-1} \sum (e_i - \bar{e})^2 \right]^{1/2} \quad (55)$$

with summation over  $n$  values  $C_{ijkl}^{exp}$  per experimental protocol.

#### 4.5.1. Ultrastructural level

Evaluation of data for various mammals (columns 3–6 of Tables 2 and 4) through Eq. (17) with  $\tilde{f}_{lac} = 2.1\%$ , Eq. (18), Eq. (20)–(28), Eq. (35)–(41) delivers composition values  $\tilde{f}_{fib}$ ,  $\tilde{f}_{HA}$ ,  $\tilde{f}_{HA}$ , and  $\tilde{f}_{col}$ , see Tables 3 and 5, corresponding to the experimental stiffness values in Fig. 6 (x-axis), see also column 8 in Tables 2 and 4. Insertion of these composition values  $\tilde{f}_{fib}$ ,  $\tilde{f}_{HA}$ ,  $\tilde{f}_{HA}$ , and  $\tilde{f}_{col}$  into Eqs. (2) to (13) delivers tissue-specific stiffness estimates  $\mathbb{C}_{ultra}^{MTII}$ . Stiffness predictions  $C_{1111}^{pred} = C_{ultra,1111}^{MTII}$  and  $C_{3333}^{pred} = C_{ultra,3333}^{MTII}$  are compared to corresponding experimental stiffness values (Fig. 6). The satisfactory agreement between model predictions and experiments is quantified by prediction errors of  $-3 \pm 14\%$  [mean value  $\pm$  standard deviation according to Eqs. (54) and (55)] for the axial (longitudinal) normal stiffness, and of  $-10 \pm 9\%$  for the radial (transverse) normal stiffness.

#### 4.5.2. Extravascular level

Evaluation of data for equine cortical bone (columns 1 and 2 of Table 6) through Eq. (19) with  $\tilde{f}_{lac} = 2.1\%$ , (29), (31), (33)–(41) delivers composition values  $\tilde{f}_{fib}$ ,  $\tilde{f}_{HA}$ ,  $\tilde{f}_{HA}$ ,  $\tilde{f}_{col}$  (see Table 7), corresponding to the experimental stiffness values labeled M90 in Fig. 7 (x-axis), see also columns 5 and 6 of Table 6. Insertion of these composition values  $\tilde{f}_{lac}$ ,  $\tilde{f}_{fib}$ ,  $\tilde{f}_{HA}$ ,  $\tilde{f}_{HA}$ , and  $\tilde{f}_{col}$  into Eqs. (2) to (14) delivers tissue-specific stiffness estimates  $\mathbb{C}_{exvas}^{MTIII}$ . Stiffness predictions  $C_{1111}^{pred} = C_{exvas,1111}^{MTIII}$  and  $C_{3333}^{pred} = C_{exvas,3333}^{MTIII}$  are compared to corresponding experimental stiffness values

labeled M90 in Fig. 7. The satisfactory agreement between model predictions and experiments is quantified by prediction errors of  $+1 \pm 22\%$  [mean value  $\pm$  standard deviation according to Eqs. (54) and (55)] for the axial (longitudinal) normal stiffness and of  $+2 \pm 30\%$  for the radial (transverse) normal stiffness.

Evaluation of data for human and bovine trabecular bone material (column 3 of Table 8) through Eq. (34) with  $\tilde{f}_{lac} = 2.1\%$ , Eq. (29), (31), (35)–(41), delivers composition values  $\tilde{f}_{fib}$ ,  $\tilde{f}_{HA}$ ,  $\tilde{f}_{HA}$ ,  $\tilde{f}_{col}$  (see Table 8), corresponding to the experimental stiffness values labeled A88 in Fig. 7 (x-axis), see also column 5 of Table 8. Insertion of these composition values  $\tilde{f}_{lac}$ ,  $\tilde{f}_{fib}$ ,  $\tilde{f}_{HA}$ ,  $\tilde{f}_{HA}$ , and  $\tilde{f}_{col}$  into Eqs. (2) to (14) delivers tissue-specific stiffness estimates  $\mathbb{C}_{exvas}^{MTIII}$ . Stiffness predictions  $C_{3333}^{pred} = C_{exvas,3333}^{MTIII}$  are compared to corresponding experimental stiffness values labeled A88 in Fig. 7. The satisfactory agreement between model predictions and experiments is quantified by prediction errors of  $+5 \pm 10\%$  [mean value  $\pm$  standard deviation according to Eqs. (54) and (55)].

Evaluation of data for a typical human femur tissue (Table 4, row 11, columns 3–6) through Eq. (17) with  $\tilde{f}_{lac} = 2.1\%$ , Eq. (18), (20), (22)–(24) delivers ultrastructural weight fractions of  $WF_{HA}^{ultra} = 0.72$  and  $WF_{org}^{ultra} = 0.24$ , typical also for the average human femoral specimen tested by Ashman et al. (1984), characterized by  $\rho_{\mu,wet} = 1.90$  g/ml (see Ashman et al., 1984, Fig. 9) and  $f_{vas} = 3\%$  (Table 4).  $WF_{HA}^{ultra}$ ,  $WF_{org}^{ultra}$ ,  $\rho_{\mu,wet}$  and  $f_{vas}$  deliver, via Eq. (17) with  $\tilde{f}_{lac} = 2.1\%$ , (18), (20), (25), (26), (35)–(41), typical composition values of  $\tilde{f}_{fib} = 0.52$ ,  $\tilde{f}_{HA} = 0.66$ ,

Table 5  
Compilation of experimental data

| Tissue          | State | $\tilde{f}_{col}$<br>(–)<br>Table 4 | $\tilde{f}_{HA}$<br>(–)<br>Table 4 | $d_s$<br>(nm)<br>Table 4 | $\tilde{f}_{fib}$<br>(–)<br>Eq. (35) | $\tilde{f}_{HA}$<br>(–)<br>Eqs. (37),<br>(39) | $\tilde{f}_{HA}$<br>(–)<br>Eqs. (37),<br>(38) | $\tilde{f}_{col}$<br>(–)<br>Eqs. (40),<br>(41) |
|-----------------|-------|-------------------------------------|------------------------------------|--------------------------|--------------------------------------|---|---|--|
| Cow tibia       | Wet   | 0.30                                | 0.48                               | 1.23                     | 0.52                                 | 0.68  | 0.29  | 0.43   |
| Cow tibia       | Wet   | 0.30                                | 0.47                               | 1.24                     | 0.52                                 | 0.68  | 0.29  | 0.42   |
| Cow tibia       | Wet   | 0.32                                | 0.44                               | 1.24                     | 0.57                                 | 0.65  | 0.28  | 0.45   |
| Cow tibia       | Wet   | 0.31                                | 0.44                               | 1.24                     | 0.55                                 | 0.65  | 0.28  | 0.44   |
| Cow tibia       | Wet   | 0.31                                | 0.45                               | 1.25                     | 0.53                                 | 0.65  | 0.28  | 0.42   |
| Cow tibia       | Wet   | 0.32                                | 0.46                               | 1.24                     | 0.55                                 | 0.68  | 0.29  | 0.44   |
| Cow tibia       | Wet   | 0.30                                | 0.49                               | 1.23                     | 0.51                                 | 0.70  | 0.29  | 0.42   |
| Cow tibia       | Wet   | 0.30                                | 0.48                               | 1.23                     | 0.52                                 | 0.69  | 0.29  | 0.43   |
| Cow tibia       | Wet   | 0.30                                | 0.48                               | 1.23                     | 0.52                                 | 0.68  | 0.29  | 0.43   |
| Elephant radius | Wet   | 0.30                                | 0.43                               | 1.26                     | 0.53                                 | 0.61  | 0.26  | 0.41   |
| Human femur     | Wet   | 0.30                                | 0.48                               | 1.26                     | 0.53                                 | 0.69  | 0.30  | 0.43   |
| Deer antler     | Wet   | 0.36                                | 0.31                               | 1.30                     | 0.66                                 | 0.49  | 0.22  | 0.47   |
| Deer antler     | Wet   | 0.37                                | 0.32                               | 1.30                     | 0.68                                 | 0.50  | 0.23  | 0.48   |
| Cow tibia       | Dry   | 0.35                                | 0.55                               | 1.17                     | 0.58                                 | 0.85  | 0.33  | 0.53   |
| Elephant radius | Dry   | 0.35                                | 0.51                               | 1.15                     | 0.57                                 | 0.78  | 0.30  | 0.50   |
| Human femur     | Dry   | 0.33                                | 0.52                               | 1.14                     | 0.52                                 | 0.77  | 0.29  | 0.46   |
| Deer antler     | Dry   | 0.44                                | 0.38                               | 1.10                     | 0.69                                 | 0.69  | 0.24  | 0.59   |
| Deer antler     | Dry   | 0.47                                | 0.40                               | 1.12                     | 0.73                                 | 0.75  | 0.27  | 0.64   |

Experimental data for ultrastructural volume fractions of hydroxyapatite and collagen,  $\tilde{f}_{HA}$  and  $\tilde{f}_{col}$ , and for the neutron diffraction spacing  $d_s$ , of various mammalian bone specimens, taken from Table 4; evaluation of experimental data for determination of ultrastructural volume fractions of fibrils,  $\tilde{f}_{fib}$ , of extrafibrillar and fibrillar volume fraction of mineral,  $\tilde{f}_{HA}$  and  $\tilde{f}_{HA}$ , and of (molecular) collagen volume fraction within the wet collagen matrix,  $\tilde{f}_{col}$ .

Table 6  
Compilation of experimental data

| $\rho_{\mu,empty}$<br>(g/cm <sup>3</sup> )<br>given | $f_{\mu por}$<br>(–)<br>given | $v_3$<br>(km/s)<br>given | $v_1$<br>(km/s)<br>given | $C_{extas,3333}^{exp}$<br>(GPa)<br>Eqs. (19) <sup>a</sup> ,<br>Eq. (33), (44) | $C_{extas,1111}^{exp}$<br>(GPa)<br>Eqs. (19) <sup>a</sup><br>Eq. (33), (42) | $f_{vas}$<br>(–)<br>Eq. (19) <sup>a</sup> | $\tilde{f}_{col}$<br>(–)<br>Eqs. (33), (34),<br>(29), (31) | $\tilde{f}_{HA}$<br>(–)<br>Eqs. (33),<br>(34), (29) | $d_s$<br>(nm)<br>Eqs. (33),<br>(34), (36) |
|---|-------------------------------|--------------------------|--------------------------|---|---|---|--|---|---|
| 2.03  | 0.10                          | 4.30                     | 3.60                     | 40.6  | 28.4  | 0.08                                      | 0.21   | 0.56  | 1.21                                      |
| 2.02  | 0.08                          | 4.20                     | 3.55                     | 37.7  | 27.0  | 0.06                                      | 0.23   | 0.53  | 1.23                                      |
| 2.01  | 0.11                          | 4.10                     | 3.45                     | 36.7  | 26.0  | 0.09                                      | 0.21   | 0.56  | 1.22                                      |
| 2.01  | 0.07                          | 4.40                     | 3.65                     | 40.8  | 28.1  | 0.05                                      | 0.25   | 0.51  | 1.23                                      |
| 2.00  | 0.09                          | 4.20                     | 3.55                     | 37.7  | 27.0  | 0.07                                      | 0.23   | 0.53  | 1.23                                      |
| 2.00  | 0.07                          | 4.20                     | 3.40                     | 37.0  | 24.2  | 0.05                                      | 0.25   | 0.50  | 1.23                                      |
| 2.00  | 0.06                          | 4.30                     | 3.58                     | 38.4  | 26.5  | 0.04                                      | 0.26   | 0.49  | 1.24                                      |
| 1.98  | 0.12                          | 4.10                     | 3.42                     | 36.7  | 25.6  | 0.10                                      | 0.21   | 0.56  | 1.22                                      |
| 1.98  | 0.12                          | 4.15                     | 3.35                     | 37.6  | 24.5  | 0.10                                      | 0.21   | 0.56  | 1.22                                      |
| 1.98  | 0.10                          | 4.15                     | 3.50                     | 36.9  | 26.2  | 0.08                                      | 0.23   | 0.53  | 1.23                                      |
| 1.98  | 0.10                          | 4.30                     | 3.60                     | 39.6  | 27.7  | 0.08                                      | 0.23   | 0.53  | 1.23                                      |
| 1.97  | 0.10                          | 4.03                     | 3.50                     | 34.5  | 26.1  | 0.08                                      | 0.24   | 0.52  | 1.23                                      |
| 1.97  | 0.12                          | 4.20                     | 3.35                     | 38.4  | 24.4  | 0.10                                      | 0.22   | 0.55  | 1.22                                      |
| 1.96  | 0.11                          | 4.03                     | 3.50                     | 34.7  | 26.2  | 0.09                                      | 0.23   | 0.53  | 1.23                                      |
| 1.96  | 0.10                          | 4.20                     | 3.60                     | 37.4  | 27.5  | 0.08                                      | 0.24   | 0.52  | 1.23                                      |
| 1.95  | 0.14                          | 3.95                     | 3.52                     | 34.3  | 27.3  | 0.12                                      | 0.21   | 0.56  | 1.21                                      |
| 1.95  | 0.09                          | 4.03                     | 3.40                     | 33.8  | 24.1  | 0.07                                      | 0.26   | 0.50  | 1.24                                      |
| 1.95  | 0.12                          | 4.10                     | 3.35                     | 36.2  | 24.2  | 0.10                                      | 0.23   | 0.54  | 1.22                                      |
| 1.95  | 0.18                          | 4.10                     | 3.42                     | 38.6  | 27.0  | 0.16                                      | 0.17   | 0.63  | 1.19                                      |
| 1.95  | 0.11                          | 4.15                     | 3.45                     | 36.5  | 25.2  | 0.09                                      | 0.24   | 0.52  | 1.23                                      |
| 1.95  | 0.14                          | 4.15                     | 3.55                     | 37.9  | 27.7  | 0.12                                      | 0.21   | 0.56  | 1.21                                      |
| 1.93  | 0.12                          | 4.03                     | 3.35                     | 34.5  | 23.9  | 0.10                                      | 0.24   | 0.52  | 1.23                                      |
| 1.93  | 0.09                          | 4.10                     | 3.30                     | 34.7  | 22.5  | 0.07                                      | 0.26   | 0.48  | 1.24                                      |
| 1.93  | 0.13                          | 4.25                     | 3.48                     | 38.9  | 26.0  | 0.11                                      | 0.23   | 0.54  | 1.22                                      |
| 1.92  | 0.12                          | 4.00                     | 3.35                     | 33.9  | 23.8  | 0.10                                      | 0.24   | 0.52  | 1.23                                      |
| 1.92  | 0.10                          | 4.03                     | 3.40                     | 33.6  | 24.0  | 0.08                                      | 0.26   | 0.49  | 1.24                                      |
| 1.92  | 0.12                          | 4.20                     | 3.35                     | 37.4  | 23.8  | 0.10                                      | 0.24   | 0.52  | 1.23                                      |
| 1.92  | 0.11                          | 4.20                     | 3.40                     | 37.0  | 24.2  | 0.09                                      | 0.25   | 0.50  | 1.23                                      |
| 1.91  | 0.12                          | 4.13                     | 3.35                     | 35.9  | 23.7  | 0.10                                      | 0.25   | 0.51  | 1.23                                      |
| 1.91  | 0.22                          | 4.17                     | 3.48                     | 41.1  | 28.5  | 0.20                                      | 0.14   | 0.66  | 1.18                                      |
| 1.91  | 0.18                          | 4.35                     | 3.45                     | 42.6  | 26.8  | 0.16                                      | 0.19   | 0.60  | 1.20                                      |
| 1.90  | 0.25                          | 3.95                     | 3.13                     | 38.0  | 23.8  | 0.23                                      | 0.11   | 0.71  | 1.17                                      |
| 1.90  | 0.12                          | 4.00                     | 3.40                     | 33.6  | 24.2  | 0.10                                      | 0.25   | 0.50  | 1.23                                      |
| 1.82  | 0.09                          | 4.00                     | 3.30                     | 31.1  | 21.2  | 0.07                                      | 0.31   | 0.41  | 1.26                                      |
| 1.76  | 0.30                          | 3.85                     | 3.20                     | 35.6  | 24.6  | 0.28                                      | 0.13   | 0.69  | 1.17                                      |

Experimental data for the microstructural mass density of tissues with empty micropores,  $\rho_{\mu,empty}$ , for the microporosity  $f_{\mu por}$ , and for the longitudinal sonic velocity in axial and in transversal direction,  $v_3$  and  $v_1$ , of equine cortical bone (McCarthy et al., 1990); evaluation of experimental data for determination of the normal stiffness component in axial and in transversal direction,  $C_{extas,3333}^{exp}$  and  $C_{extas,1111}^{exp}$ , of ultrastructural volume fractions of hydroxyapatite and collagen,  $\tilde{f}_{HA}$  and  $\tilde{f}_{col}$ , as well as of the neutron diffraction spacing  $d_s$ .

<sup>a</sup>Computed with  $\tilde{f}_{lac} = 2.1\%$ , according to Eq. (17), with  $f_{lac} = 2\%$  and  $f_{vas} = 3\%$ , determined from micrograph of Fig. 1(c) on the basis of Eqs. (15) and (16).

$\tilde{f}_{HA} = 0.29$ , and  $\tilde{f}_{col} = 0.41$ . Insertion of these composition values  $\tilde{f}_{lac}$ ,  $\tilde{f}_{fib}$ ,  $\tilde{f}_{HA}$ ,  $\tilde{f}_{HA}$ , and  $\tilde{f}_{col}$  into Eqs. (2) to (14) delivers a stiffness estimate (model prediction) of

$$\mathbb{C}_{extas}^{MTIII} = \begin{pmatrix} 18.3 & 8.1 & 8.1 & 0 & 0 & 0 \\ 8.1 & 18.3 & 8.1 & 0 & 0 & 0 \\ 8.1 & 8.1 & 28.4 & 0 & 0 & 0 \\ 0 & 0 & 0 & 12.5 & 0 & 0 \\ 0 & 0 & 0 & 0 & 12.5 & 0 \\ 0 & 0 & 0 & 0 & 0 & 10.1 \end{pmatrix}. \quad (56)$$

We observe a good agreement of this prediction with experimental values of Eq. (53), being quantified by relative

prediction errors of  $\pm 0\%$  for  $C_{3333}$ ,  $-7\%$  for  $C_{1111}$ ,  $3\%$  for  $C_{1313}$  and  $9\%$  for  $C_{1212}$ .

## 5. Discussion

This contribution aimed at quantification of the mechanical effects of universal patterns across different extra-vascular and extracellular cortical and trabecular bone materials. Such patterns have been identified across the hierarchical organization of bone materials; from typical pore shapes in the micrometer to millimeter regime down to the level of the elementary constituents of bone, namely mineral crystals, collagen molecules, and water.



Table 7  
Compilation of experimental data

| $\tilde{f}_{col}$<br>(–)<br>Table 6 | $\tilde{f}_{HA}$<br>(–)<br>Table 6 | $d_s$<br>(nm)<br>Table 6 | $\tilde{f}_{fib}$<br>(–)<br>Eq. (35) | $\tilde{f}_{HA}$<br>(–)<br>Eqs. (37),<br>(39) | $\tilde{f}_{HA}$<br>(–)<br>Eqs. (37),<br>(38) | $\tilde{f}_{col}^{\circ}$<br>(–)<br>Eqs. (40),<br>(41) |
|-------------------------------------|------------------------------------|--------------------------|--------------------------------------|---|---|--|
| 0.21                                | 0.56                               | 1.21                     | 0.36                                 | 0.71  | 0.29  | 0.30   |
| 0.23                                | 0.53                               | 1.23                     | 0.40                                 | 0.69  | 0.29  | 0.33   |
| 0.21                                | 0.56                               | 1.22                     | 0.37                                 | 0.71  | 0.29  | 0.30   |
| 0.25                                | 0.51                               | 1.23                     | 0.43                                 | 0.68  | 0.28  | 0.34   |
| 0.23                                | 0.53                               | 1.23                     | 0.40                                 | 0.69  | 0.29  | 0.33   |
| 0.25                                | 0.50                               | 1.23                     | 0.43                                 | 0.67  | 0.28  | 0.35   |
| 0.26                                | 0.49                               | 1.24                     | 0.45                                 | 0.66  | 0.28  | 0.36   |
| 0.21                                | 0.56                               | 1.22                     | 0.36                                 | 0.71  | 0.29  | 0.30   |
| 0.21                                | 0.56                               | 1.22                     | 0.36                                 | 0.71  | 0.29  | 0.30   |
| 0.23                                | 0.53                               | 1.23                     | 0.40                                 | 0.69  | 0.29  | 0.33   |
| 0.23                                | 0.53                               | 1.23                     | 0.40                                 | 0.69  | 0.29  | 0.33   |
| 0.24                                | 0.52                               | 1.23                     | 0.41                                 | 0.69  | 0.29  | 0.33   |
| 0.22                                | 0.55                               | 1.22                     | 0.37                                 | 0.70  | 0.29  | 0.31   |
| 0.23                                | 0.53                               | 1.23                     | 0.40                                 | 0.69  | 0.29  | 0.33   |
| 0.24                                | 0.52                               | 1.23                     | 0.42                                 | 0.68  | 0.29  | 0.34   |
| 0.21                                | 0.56                               | 1.21                     | 0.35                                 | 0.71  | 0.29  | 0.30   |
| 0.26                                | 0.50                               | 1.24                     | 0.44                                 | 0.67  | 0.28  | 0.36   |
| 0.23                                | 0.54                               | 1.22                     | 0.39                                 | 0.69  | 0.29  | 0.32   |
| 0.17                                | 0.63                               | 1.19                     | 0.28                                 | 0.75  | 0.30  | 0.24   |
| 0.24                                | 0.52                               | 1.23                     | 0.42                                 | 0.68  | 0.29  | 0.34   |
| 0.21                                | 0.56                               | 1.21                     | 0.35                                 | 0.71  | 0.29  | 0.30   |
| 0.24                                | 0.52                               | 1.23                     | 0.41                                 | 0.69  | 0.29  | 0.33   |
| 0.26                                | 0.48                               | 1.24                     | 0.46                                 | 0.66  | 0.28  | 0.37   |
| 0.23                                | 0.54                               | 1.22                     | 0.39                                 | 0.70  | 0.29  | 0.32   |
| 0.24                                | 0.52                               | 1.23                     | 0.42                                 | 0.68  | 0.29  | 0.34   |
| 0.26                                | 0.49                               | 1.24                     | 0.45                                 | 0.66  | 0.28  | 0.36   |
| 0.24                                | 0.52                               | 1.23                     | 0.42                                 | 0.68  | 0.29  | 0.34   |
| 0.25                                | 0.50                               | 1.23                     | 0.43                                 | 0.67  | 0.28  | 0.35   |
| 0.25                                | 0.51                               | 1.23                     | 0.42                                 | 0.68  | 0.28  | 0.34   |
| 0.14                                | 0.66                               | 1.18                     | 0.24                                 | 0.77  | 0.31  | 0.21   |
| 0.19                                | 0.60                               | 1.20                     | 0.31                                 | 0.73  | 0.30  | 0.27   |
| 0.11                                | 0.71                               | 1.17                     | 0.18                                 | 0.80  | 0.31  | 0.16   |
| 0.25                                | 0.50                               | 1.23                     | 0.43                                 | 0.67  | 0.28  | 0.35   |
| 0.31                                | 0.41                               | 1.26                     | 0.55                                 | 0.60  | 0.26  | 0.42   |
| 0.13                                | 0.69                               | 1.17                     | 0.21                                 | 0.79  | 0.31  | 0.18   |

Experimental data of ultrastructural volume fractions of hydroxyapatite and collagen,  $\tilde{f}_{HA}$  and  $\tilde{f}_{col}$ , as well as of neutron diffraction spacing  $d_s$ , taken from Table 6; evaluation of experimental data for determination of ultrastructural volume fractions of fibrils,  $\tilde{f}_{fib}$ , of extrafibrillar and fibrillar volume fraction of mineral,  $\tilde{f}_{HA}$  and  $\tilde{f}_{HA}^{\circ}$ , and of (molecular) collagen volume fraction within the wet collagen matrix,  $\tilde{f}_{col}^{\circ}$ .

### 5.1. Mineral-collagen interactions

Collagen molecules self-assemble into staggered schemes called fibrils, held together by crosslinks. Impure hydroxyapatite crystals precipitate inside these fibrils (intrafibrillar bone mineral) and between these fibrils (interfibrillar mineral). We have modeled the mechanical effects of these arrangements by means of a micromechanical representation comprising three homogenization steps [Fig. 3(a, b, d)]: (i) crosslinked collagen molecules form a wet-collagen-matrix [Fig. 3(a)], (ii) wet-collagen-matrix and mineral agglomerations penetrate each other to form the so called mineralized fibril [Fig. 3(b)], (iii) mineralized fibrils are embedded in an extrafibrillar mineral foam matrix [Fig. 3(d)].

This representation deserves a discussion with respect to the pertinent literature on the topic: All three steps are in agreement with well-documented ideas; namely those of (i) collagen molecules forming a contiguous matrix (Currey, 1969; Katz, 1980, 1981; Sasaki, 1991; Mammone and Hudson, 1993; Jäger and Fratzl, 2000; Kotha and Guzelsu, 2003); (ii) collagen and mineral interpenetrating each other (Benezra Rosen et al., 2002; Currey, 2003; Hellmich et al., 2004a); and (iii) mineral crystals forming a contiguous matrix (Crolet et al., 1993; Aoubiza et al., 1996; Benezra Rosen et al., 2002; Hellmich and Ulm, 2002a; Wang and Qian, 2006). While a choice for *one* of these different concepts seemed unavoidable in the aforementioned references, we here propose a reconciliation of all three, assigning each idea to another observation scale: the first one to  $\approx 10$  nm, the second one to several hundred nanometers, and the third one to 5–10  $\mu$ m.

Apart from the appealing feature that none of the above referenced, well-argued ideas on mineral–collagen interaction has to be rejected in the present approach, there is a strong quantitative argument for it: the low relative errors between stiffness experiments at different observation scales and corresponding stiffness predictions by a model which is based on measured tissue-independent stiffnesses of the elementary constituents of bone (collagen, hydroxyapatite, water), on their tissue-dependent experimentally determined dosages, and their ‘universal’ interaction patterns; notably, the model does not involve material parameters which need to be guessed or back-analysed. If these low prediction errors undercut the ones of any other model having undergone a comparably strict validation procedure, then the present model is superior to those other strictly validated models, such as the recent proposals of Hellmich et al. (2004a); Hellmich (2005) on the micromechanical representation of the mineralized collagen fibril, where minerals and collagen molecules interact directly at the length scale of several nanometers. Indeed, the 59% of prediction error (Hellmich, 2005) in anisotropic shear stiffness of cortical bone material encountered in the aforementioned approach (being, by the way, satisfactory for normal stiffness components) is clearly undercut by the 9% encountered herein (see Section 4).

This motivates a short re-consideration of typical dimensions of collagen molecules, mineral crystals, collagen and mineral assemblies, and mineralized fibrils: In fact, the thickness of hydroxyapatite crystals, recently given as 2 nm (Eppell et al., 2001; Tong et al., 2003) is well comparable to that of the diameter of collagen molecule, amounting to about 1 nm (Miller, 1984; Lees et al., 1984b; Lees, 1987); this would support introduction of collagen, mineral and water phases in one and the same representative volume element, as done in Hellmich et al. (2004a); Hellmich (2005). However, a closer look onto the three dimensional arrangement of collagen molecules and mineral crystals reveals the relevance of our present approach: In a cross section through a fibril,  $\approx 1$  nm thick cylindrical collagen molecules form (on average) an

Table 8  
Compilation of experimental data

| Tissue       | State | $\rho_{\text{exvas}}$<br>(g/cm <sup>3</sup> )<br>given | $v_3$<br>(km/s)<br>given | $C_{\text{exvas},3333}^{\text{exp}}$<br>(GPa)<br>Eq. (44) | $\tilde{f}_{\text{col}}$<br>(–)<br>Eqs. (34) <sup>a</sup> ,<br>(29), (31) | $\tilde{f}_{\text{HA}}$<br>(–)<br>Eqs. (34) <sup>a</sup> ,<br>(29) | $d_s$<br>(nm)<br>Eqs. (34) <sup>a</sup> ,<br>(36) | $\tilde{f}_{\text{fib}}$<br>(–)<br>Eq. (35) | $\tilde{f}_{\text{HA}}$<br>(–)<br>Eqs. (37),<br>(39) | $\tilde{f}_{\text{HA}}$<br>(–)<br>Eqs. (37),<br>(38) | $\tilde{f}_{\text{col}}$<br>(–)<br>Eqs. (40),<br>(41) |
|--------------|-------|--|--------------------------|---|---|--|---|---|--|--|---|
| Human femur  | Wet   | 1.80   | 2.64                     | 12.6  | 0.37  | 0.33   | 1.29  | 0.67  | 0.52   | 0.23   | 0.48  |
| Human femur  | Wet   | 1.78   | 2.72                     | 13.2  | 0.38  | 0.31   | 1.30  | 0.70  | 0.50   | 0.23   | 0.49  |
| Human femur  | Wet   | 1.73   | 2.75                     | 13.1  | 0.40  | 0.28   | 1.31  | 0.74  | 0.47   | 0.21   | 0.51  |
| Bovine femur | Wet   | 1.74   | 2.50                     | 10.9  | 0.40  | 0.29   | 1.31  | 0.73  | 0.48   | 0.22   | 0.51  |

Experimental data for the extravascular mass density of tissues with empty micropores,  $\rho_{\text{exvas}}$ , and for the longitudinal sonic velocity in axial direction,  $v_3$ , of human and bovine trabecular bone (Ashman and Rho, 1988); evaluation of experimental data for determination of the normal stiffness component in axial direction,  $C_{\text{exvas},3333}^{\text{exp}}$ , of ultrastructural volume fractions of hydroxyapatite and collagen,  $\tilde{f}_{\text{HA}}$  and  $\tilde{f}_{\text{col}}$ , of the neutron diffraction spacing  $d_s$ , of ultrastructural volume fraction of fibrils,  $\tilde{f}_{\text{fib}}$ , of extrafibrillar and fibrillar volume fraction of mineral,  $\tilde{f}_{\text{HA}}$  and  $\tilde{f}_{\text{HA}}$ , as well as of (molecular) collagen volume fraction within the wet collagen matrix,  $\tilde{f}_{\text{col}}$ .

<sup>a</sup>Computed with  $\tilde{f}_{\text{lac}} = 2.1\%$ , according to Eq. (17), with  $f_{\text{lac}} = 2\%$  and  $f_{\text{vas}} = 3\%$ , determined from micrograph of Fig. 1(c) on the basis of Eqs. (15) and (16).

hexagonal pattern (Lees et al., 1984b; Miller, 1984) with about 1 nm intermolecular distance. Transmission electron microscopy, however, revealed single hydroxyapatite crystals to exceed several nanometers length in at least *two* dimensions; forming plates with typically 25 nm width and 50 nm length (Weiner and Wagner, 1998). In addition, these crystals tend to be connected to each other (Benezra Rosen et al., 2002), forming agglomerations or clusters measuring tens to hundreds of nanometers (Landis et al., 1993, 1996; Zylberberg et al., 1998; Hassenkam et al., 2004): Hence, in the fibril cross section, crystals and crystal clusters are clearly separated by scale from the collagen molecules, as it is accounted for in the present approach [Fig. 3(a) and (b)]. At the same time, the very long extension of the collagen molecules in fibrillar direction is properly considered through the infinitely long cylindrical collagen inclusions [Fig. 3(b)].

### 5.2. Porous hydroxyapatite polycrystals

The large amounts of hydroxyapatite present *outside* the collagen fibrils were first evidenced by Transmission Electron Microscopy (Lees et al., 1994b; Probst and Lees, 1996; Zylberberg et al., 1998), then corroborated by mechanical modeling (Pidaparti et al., 1996), and finally quantified to comprise between 60% and almost 100% of the entire bone mineral, depending on the considered tissue (Hellmich and Ulm, 2001; Sasaki et al., 2002; Hellmich and Ulm, 2003). In de-organifying experiments (Benezra Rosen et al., 2002) these crystals have been shown to form, with a highly random orientation distribution (Fratzl et al., 1996; Peters et al., 2000), a contiguous network, which acts mechanically as a mineral foam (Hellmich and Ulm, 2002a) or porous polycrystal (Hellmich and Ulm, 2002b; Hellmich et al., 2004a; Fritsch et al., 2006). Micromechanical representation of this material type by isotropic mineral and nanopore spheres in an effective matrix with the homogenized polycrystal properties [Section 3.3, Fig. 3(c)]

was strongly supported by experimental data (Hellmich and Ulm, 2002a; Hellmich et al., 2004b), but might still seem somewhat simplistic with regards to two aspects: (i) The crystal structure of hydroxyapatite suggests anisotropic mechanical behavior; (ii) the crystals are not spherical, but rather plate-shaped (Eppell et al., 2001; Tong et al., 2003; Su et al., 2003; Hassenkam et al., 2004). As for hydroxyapatite anisotropy, we note that only the isotropic elastic properties of biologically generated hydroxyapatite could be revealed from ultrasonic tests on powder (Gilmore and Katz, 1982), and that the anisotropy of hydroxyapatite can only be estimated from the experimentally accessible anisotropy of a very similar crystal, fluorapatite (Katz and Ukraincik, 1971). Given the recent finding of Jäger et al. (2006) that the surface of hydroxyapatite grown in quasi-biological conditions is in fact amorphous (with consequently isotropic behavior), Katz’s anisotropy estimate turns out to be an upper bound for the anisotropy of hydroxyapatite, while indeed isotropy of hydroxyapatite may be encountered in mineralized tissues. In the same sense, crystal needles might be regarded as morphological opposite of spheres, with the ‘real’ crystal shape lying between these two extremes. Remarkably, a micromechanical model with anisotropic crystal needles instead of isotropic spheres (Fritsch et al., 2006) predicts, for physiologically relevant mineral concentrations, effective stiffnesses which are quasi-identical to those of the model in Section 3.3 and Fig. 3(c): This further corroborates the relevance of the herein used micromechanical representation of the extrafibrillar space.

### 5.3. Fibril orientation

Throughout our herein presented developments, we consider parallel-oriented collagen fibrils: We first introduce this orientation within an RVE of 5–10 μm characteristic length [see Fig. 3(d)]. Such parallel orientation of fibrils at this length scale was evidenced in numerous

mineralized tissues (horse radius, Raspanti et al., 1995, 1996, normal and osteoporotic human trabecular bone (Rubin et al., 2003), human tibial bone (Prostak and Lees, 1996), bovine trabecular vertebral bone (Hassenkam et al., 2004), bovine tibial cortical bone (Tai et al., 2005), bovine femoral cortical bone (Sasaki et al., 2002), and mineralized turkey leg tendon (Lees et al., 1994b)) through several experimental techniques, such as scanning electron microscopy (SEM) (Raspanti et al., 1996, 1995, Tai et al., 2005) Transmission Electron Microscopy (TEM) (Lees et al., 1994b; Prostak and Lees, 1996; Rubin et al., 2003), and Atomic Force Microscopy (AFM) (Lees et al., 1994b; Sasaki et al., 2002; Hassenkam et al., 2004; Tai et al., 2005). This parallel organization can be destroyed by reorientation of collagen fibrils during demineralization (Raspanti et al., 1996; Rubin et al., 2004; Tai et al., 2005), which may lead to an even isotropic material behavior of the demineralized tissue (Hasegawa et al., 1994). The aforementioned parallel orientation of collagen fibrils in mineralized tissues may be maintained up to the observation scale of several hundred micrometers, as evidenced by Riggs et al. (1993) and Raspanti et al. (1996) for the cranial (anterior) cortex of the equine radius, through circular-polarized light microscopy and SEM, respectively. This is in perfect agreement with our homogenization steps of Fig. 3(d) and (e). However, at this observation scale of hundred micrometers, sometimes remarkable deviations of collagen fibril orientation from a single direction may be found, e.g. in the posterior part of equine radii (Raspanti et al., 1996; Riggs et al., 1993). In case such tissues were to be analysed by our micromechanical approach, the homogenization step of Fig. 3(d) might be to be modified, on the basis of orientation information gained from microscopy.

The deviation of fibrillar orientation from the anatomical axis is often referred to in the context of concentric layers (lamellae) forming a secondary osteon around a Haversian canal. Numerous authors agree that the appearance of these lamellae in a cross section seen under polarized light microscopy (PLM) indicates the fibrillar orientation within these layers (Gebhardt, 1906; Ascenzi and Bonucci, 1968; Black et al., 1974; Reid, 1986; Giraud-Guille, 1988; Riggs et al., 1993). Dark appearance of lamellae refers to longitudinal collagen fibril orientation, whereas bright appearance indicates a certain deviation of the fibrils from the longitudinal axis (as confirmed, through SEM, by Frasca et al., 1977). However, the thickness of 'bright' lamellae is overestimated by PLM, as was shown by comparison of PLM-images to electron micrographs (SEM as well as TEM) (Reid, 1986, p. 332), (Marotti, 1993, p. S51). Hence, the majority of collagen fibrils in secondary osteons seems to be longitudinally oriented, as modeled in our homogenization step of Fig. 3(d). In particular, the tissues used for model validation in Section 4.4.2, such as human tibial bone, are probable to show collagen fibril and fiber arrangement more or less parallel to the long bone axis, as evidenced by the TEM-images of Prostak and Lees

(1996); Rubin et al. (2003). Still, it is interesting to study the effect of collagen fibril deviation from the longitudinal direction in the bright lamellae, evidenced e.g. through SEM as amounting to around  $\pm 20^\circ$ , see (Raspanti et al., 1995, 1996). If we simply allow the collagen fibrils to be axisymmetrically oriented with a uniform deviation distribution between  $0^\circ$  and  $20^\circ$  (see Fritsch et al., 2006 for mathematical implications), while neglecting, due to the lack of precise geometrical information on the tissues used for model validation, the actual sequence of lamellae, the corresponding micromechanical predictions are still characterized by a mean relative error of at most 10%. This seems to corroborate an earlier statement (quoted from Riggs et al. (1993, p. 245)) that '... the presence or absence of secondary osteons has per se little influence on the mechanical properties of bone'. In summary, the present consideration of collagen fibril orientation in the micromechanical explanation of the elastic anisotropy of extravascular and extracellular bone materials may well be regarded as satisfying, unless the state of completeness in experimental characterization of geometrical and elastic properties across the hierarchical organization of bone might be further improved in the future.

#### 5.4. Vascular pore spaces

Herein, we limit our presentation to observation scales of at most  $100\text{ }\mu\text{m}$ , i.e. to analysis of cortical and trabecular bone material including lacunar porosity. Homogenization of the vascular porosity (Haversian and Volkmann canals in cortical bone, intertrabecular space in trabecular bone) within an additional RVE of one to several millimeters characteristic length is an open challenge, if the aforementioned prediction errors of at most 10% (compare (Hellmich, 2005)) shall not be exceeded. This is particularly true for trabecular bone: If we represent intertrabecular porosity simply through cylindrical pores (as proposed by Hellmich et al., 2004b), we face prediction errors of typically 15% to 20%, both for normal and shear stiffness properties. Remarkably, this is still more than one order of magnitude more precise than pertinent trabecular homogenization strategies (Hollister et al., 1991, 1994); and, as regards shear stiffness, prediction errors related to our earlier model propositions (Hellmich, 2005), amounting up to 64%, are clearly undercut. Nevertheless, we plan to further reduce the aforementioned prediction errors of 15–20%, by refining the micromechanical representation of trabecular microarchitecture, beyond the one of cylindrical pores in an extravascular bone matrix. Alternatively, it might be worthwhile to combine the herein presented, reasonably precise anisotropic and inhomogeneous stiffness estimates for extravascular bone material [Fig. 3(a)–(e)] with detailed microstructural modeling of the trabecular microarchitecture in the framework of micro finite element modeling ( $\mu\text{FEM}$ ), pioneered by (Rietbergen et al., 1995) and widely available nowadays. Such a combination may have the potential to overcome both

the aforementioned limitations of continuum micromechanics representations for bone microstructure and those of contemporary  $\mu$ -FE-analysis, characterized by isotropic properties of (extravascular) solid bone material. The latter limitations have been recently evidenced by 3D digital volume correlation measurements (Zaue et al., 2006).

### 5.5. Conclusions and perspectives

We have provided evidence for common ('universal') mechanical interaction patterns in a variety of bone materials, through development of a multiscale material law and its validation by independent experimental sets at the extracellular and extravascular observation scales: Tissue-specific stiffness values predicted by the micromechanical model on the basis of tissue-independent ('universal') stiffnesses of the elementary components (mineral, collagen, water), for tissue-specific composition data (volume fractions) were compared to corresponding experimentally determined tissue-specific stiffness values. Mean relative errors between stiffness experiments and model estimates did not exceed 10%, which reflects a predictive precision which—to the knowledge of the authors—has never been attained so far. Thanks to these characteristics, the model allows for translation of non-invasively accessible composition data obtainable from computer tomography (CT), such as volumetric bone mineral density (vBMD) (Lang et al., 1997, 2002; Neu et al., 2001; Wachter et al., 2001) and bone volume over total volume (BV/TV) (Müller et al., 1996; Wachter et al., 2001), via  $f_{\mu por} = 1 - BV/TV$ ,  $\bar{f}_{HA} = vBMD \times BV/TV$ , and  $\bar{f}_{col}$  according to Eq. (31) and Fig. 4, into tissue-specific anisotropic elasticity tensors; following the line proposed by Torabia (2004); Torabia and Hellmich (2004). This opens new possibilities in the exploitation of computer tomographic data for nano-to-macro mechanics of bone organs, especially in combination with currently investigated extensions towards damage and failure. Recently, corresponding theoretical formulations proposed by Kreher (1990); Kreher and Molinari (1993); Dormieux et al. (2002); Barthélémy and Dormieux (2003) have been successfully applied to another class of biological materials, wood (Hofstetter et al. 2005a, b). As regards other current research directions, it is important to recall that micro-mechanical formulations such as the one presented here give direct access to fluid pressures in pore spaces and to poroelastic properties in general (Hellmich and Ulm, 2005a, b), crucial for cell nutrition (Knothe Tate, 2003) and bone adaptation (Cowin, 1999).

### Acknowledgments

This work was supported in part by the EU Network of Excellence project Knowledge-based Multicomponent Materials for Durable and Safe Performance (KMM-NoE) under the contract no. NMP3-CT-2004-502243.

### Appendix A. Hill tensor $\mathbb{P}$ for spherical inclusions in a transversely isotropic matrix

The components of the Hill tensor  $\mathbb{P}$  for spherical inclusions in a transversely isotropic matrix are given in (Hellmich et al., 2004a) and read as:

$$\begin{aligned} P_{sph,1111}^0 = & \frac{1}{16} \int_{-1}^1 (-5C_{1111}^0 x^4 C_{3333}^0 - 3C_{1122}^0 x^2 C_{3333}^0 \\ & - 3C_{1122}^0 x^4 C_{2323}^0 \\ & + 3C_{1122}^0 x^4 C_{3333}^0 + 5C_{1111}^0 x^4 C_{2323}^0 \\ & - 10C_{1111}^0 C_{2323}^0 x^2 + 2x^4 C_{1133}^{0,2} \\ & + 8C_{2323}^0 x^4 C_{3333}^0 - 6C_{2323}^{0,2} x^4 \\ & + 4C_{2323}^0 x^4 C_{1133}^0 + 6C_{1122}^0 C_{2323}^0 x^2 \\ & + 5C_{1111}^0 C_{2323}^0 + 5C_{1111}^0 x^2 C_{3333}^0 \\ & - 4C_{2323}^0 x^2 C_{1133}^0 + 6C_{2323}^{0,2} x^2 \\ & - 2x^2 C_{1133}^{0,2} - 3C_{1122}^0 C_{2323}^0) \\ & \times (-1 + x^2) / \mathcal{D}_1 dx, \end{aligned} \quad (A.1)$$

$$\begin{aligned} P_{sph,1122}^0 = & P_{sph,2211}^0 \\ = & \frac{1}{16} \int_{-1}^1 (C_{1111}^0 C_{2323}^0 - 2C_{1111}^0 C_{2323}^0 x^2 \\ & + C_{1111}^0 x^2 C_{3333}^0 + C_{1122}^0 C_{2323}^0 \\ & - 2C_{1122}^0 C_{2323}^0 x^2 + C_{1122}^0 x^2 C_{3333}^0 \\ & + C_{1111}^0 x^4 C_{2323}^0 - C_{1111}^0 x^4 C_{3333}^0 \\ & + C_{1122}^0 x^4 C_{2323}^0 - C_{1122}^0 x^4 C_{3333}^0 - 2C_{2323}^{0,2} x^2 \\ & + 2C_{2323}^{0,2} x^4 - 4C_{2323}^0 x^2 C_{1133}^0 \\ & + 4C_{2323}^0 x^4 C_{1133}^0 - 2x^2 C_{1133}^{0,2} \\ & + 2x^4 C_{1133}^{0,2}) (-1 + x^2) / \mathcal{D}_1 dx, \end{aligned} \quad (A.2)$$

$$\begin{aligned} P_{sph,1133}^0 = & P_{sph,3311}^0 \\ = & \frac{1}{4} \int_{-1}^1 (-1 + x^2) x^2 (C_{2323}^0 + C_{1133}^0) / \mathcal{D}_2 dx, \end{aligned} \quad (A.3)$$

$$\begin{aligned} P_{sph,2323}^0 = & \frac{1}{16} \int_{-1}^1 (4C_{1111}^0 C_{2323}^0 x^2 - 8C_{2323}^0 x^4 C_{1133}^0 \\ & - 2x^4 C_{1133}^{0,2} - C_{1122}^0 x^4 C_{3333}^0 \\ & - 8C_{1111}^0 x^4 C_{2323}^0 + 3C_{1111}^0 x^4 C_{3333}^0 \\ & + 4C_{1111}^0 x^4 C_{1133}^0 - 4C_{1122}^0 x^4 C_{1133}^0 \\ & + 2C_{1122}^0 x^6 C_{1133}^0 - 2C_{1111}^0 x^6 C_{1133}^0 \\ & + C_{1122}^0 x^6 C_{1111}^0 - 3C_{1122}^0 x^4 C_{1111}^0 \\ & + 3C_{1122}^0 C_{1111}^0 x^2 - 2C_{1111}^0 x^2 C_{1133}^0 \\ & + 2C_{1122}^0 x^2 C_{1133}^0 + 8x^6 C_{2323}^0 C_{1133}^0 \\ & - 3x^6 C_{1111}^0 C_{3333}^0 + 4x^6 C_{2323}^0 C_{3333}^0) \end{aligned}$$



$$\begin{aligned}
& + 4C_{1111}^0 x^6 C_{2323}^0 + C_{1122}^0 x^6 C_{3333}^0 \\
& + 3C_{1111}^{0,2} x^4 - C_{1111}^{0,2} x^6 \\
& + 2C_{1133}^{0,2} x^6 - 3C_{1111}^{0,2} x^2 \\
& + C_{1111}^{0,2} - C_{1122}^0 C_{1111}^0) / \mathcal{D}_1 dx, \quad (A.4)
\end{aligned}$$

$$\begin{aligned}
P_{sph,3333}^0 = & \frac{1}{2} \int_{-1}^1 x^2 (x^2 C_{2323}^0 - C_{1111}^0 x^2 \\
& + C_{1111}^0) / \mathcal{D}_2 dx, \quad (A.5)
\end{aligned}$$

whereby

$$\begin{aligned}
\mathcal{D}_1 = & -2C_{1111}^{0,2} x^4 C_{3333}^0 + 2C_{2323}^{0,2} x^6 C_{3333}^0 - 4C_{1111}^0 C_{2323}^{0,2} x^4 \\
& - 3C_{1111}^{0,2} C_{2323}^0 x^2 + C_{1111}^{0,2} x^2 C_{3333}^0 \\
& + 2C_{1111}^0 C_{2323}^{0,2} x^2 - 2C_{2323}^0 x^4 C_{1133}^{0,2} - C_{1111}^0 C_{1133}^{0,2} x^6 \\
& + 2C_{1111}^0 C_{1133}^{0,2} x^4 + 4C_{2323}^{0,2} x^6 C_{1133}^0 \\
& - 2C_{1122}^0 C_{1133}^{0,2} x^4 + 2C_{2323}^0 x^6 C_{1133}^{0,2} + 3C_{1111}^{0,2} x^4 C_{2323}^0 \\
& + C_{1122}^0 C_{1133}^{0,2} x^6 - C_{1111}^{0,2} x^6 C_{2323}^0 \\
& + 2C_{1111}^0 x^6 C_{2323}^{0,2} + C_{1111}^{0,2} x^6 C_{3333}^0 - C_{1111}^0 C_{1133}^{0,2} x^2 \\
& - 4C_{2323}^{0,2} x^4 C_{1133}^0 + C_{1122}^0 C_{1133}^{0,2} x^2 \\
& + C_{1111}^{0,2} C_{2323}^0 - C_{1122}^0 C_{1111}^0 C_{2323}^0 - C_{1122}^0 x^6 C_{1111}^0 C_{3333}^0 \\
& + 4C_{1111}^0 x^4 C_{2323}^0 C_{1133}^0 - 2C_{1111}^0 x^2 C_{2323}^0 C_{1133}^0 \\
& - 4C_{1122}^0 x^4 C_{2323}^0 C_{1133}^0 + 2C_{1122}^0 x^2 C_{2323}^0 C_{1133}^0 \\
& + 2C_{1122}^0 x^6 C_{2323}^0 C_{1133}^0 - 2C_{1111}^0 x^6 C_{2323}^0 C_{1133}^0 \\
& - 3C_{1111}^0 x^6 C_{2323}^0 C_{3333}^0 + 2C_{1122}^0 C_{1111}^0 x^4 C_{3333}^0 \\
& - C_{1122}^0 C_{2323}^0 x^4 C_{3333}^0 - 3C_{1122}^0 C_{1111}^0 x^4 C_{2323}^0 \\
& - C_{1122}^0 C_{1111}^0 x^2 C_{3333}^0 + 3C_{1122}^0 C_{1111}^0 C_{2323}^0 x^2 \\
& + 3C_{1111}^0 C_{2323}^0 x^4 C_{3333}^0 + C_{1122}^0 x^6 C_{1111}^0 C_{2323}^0 \\
& + C_{1122}^0 x^6 C_{2323}^0 C_{3333}^0 \quad (A.6)
\end{aligned}$$

and

$$\begin{aligned}
\mathcal{D}_2 = & 2C_{2323}^0 x^4 C_{1133}^0 + C_{2323}^0 x^4 C_{3333}^0 + C_{1111}^0 x^4 C_{2323}^0 \\
& - 2C_{2323}^0 x^2 C_{1133}^0 - 2C_{1111}^0 C_{2323}^0 x^2 \\
& + C_{1111}^0 C_{2323}^0 + x^4 C_{1133}^{0,2} - C_{1111}^0 x^4 C_{3333}^0 \\
& - x^2 C_{1133}^{0,2} + C_{1111}^0 x^2 C_{3333}^0. \quad (A.7)
\end{aligned}$$

These integral expressions are evaluated numerically, based on an adaptive Simpson quadrature, which is standardly available in MATLAB (Hunt et al., 2001).

## References

- Aoubiza, B., Crolet, J., Meunier, A., 1996. On the mechanical characterization of compact bone structure using homogenization theory. *J. Biomech.* 29 (6), 1539–1547.
- Ascenzi, A., Bonucci, E., 1968. The compressive properties of single osteons. *Anat. Rec.* 161 (3), 377–392.
- Ashman, R., Rho, J., 1988. Elastic modulus of trabecular bone material. *J. Biomech.* 21 (3), 177–181.
- Ashman, R., Cowin, S., van Buskirk, W., Rice, J., 1984. A continuous wave technique for the measurement of the elastic properties of cortical bone. *J. Biomech.* 17 (5), 349–361.
- Bailey, A., Paul, R., Knott, L., 1998. Mechanisms of maturation and ageing of collagen. *Mech. Ageing Develop.* 106, 1–56.
- Barthélémy, J.-F., Dormieux, L., 2003. Determination of the macroscopic strength criterion of a porous medium by nonlinear homogenization. *C. R. Mec.* 331, 271–276.
- Baylink, D., Wergedal, J., 1971. Bone Formation and Resorption by Osteocytes. Academic Press, New York, USA, pp. 257–289.
- Benezra Rosen, V., Hobbs, L., Spector, M., 2002. The ultrastructure of anorganic bovine bone and selected synthetic hydroxyapatites used as bone graft substitute material. *Biomaterials* 23, 921–928.
- Black, J., Mattson, R., Korostoff, E., 1974. Haversian osteons: Size, distribution, internal structure, and orientation. *J. Biomed. Mater. Res.* 8, 299–319.
- Bonar, L., Lees, S., Mook, H., 1985. Neutron diffraction studies of collagen in fully mineralized bone. *J. Mol. Biol.* 181, 265–270.
- Bowman, S., Zeind, J., Gibson, L., Hayes, W., McMahon, T., 1996. The tensile behavior of demineralized bovine cortical bone. *J. Biomech.* 29 (11), 1497–1501.
- Catanese, J., Iverson, E., Ng, R., Keaveny, T., 1999. Heterogeneity of the mechanical properties of demineralized bone. *J. Biomech.* 32, 1365–1369.
- Christiansen, D., Huang, E., Silver, F., 2000. Assembly of type I collagen: fusion of fibril subunits and the influence of fibril diameter on mechanical properties. *Matrix Biol.* 19, 409–420.
- Cowin, S., 1999. Bone poroelasticity. *J. Biomech.* 32, 217–238.
- Crolet, J., Aoubiza, B., Meunier, A., 1993. Compact bone: numerical simulation of mechanical characteristics. *J. Biomech.* 26 (6), 677–687.
- Currey, J., 1969. The relationship between the stiffness and the mineral content of bone. *J. Biomech.* 2, 477–480.
- Currey, J., 2003. Role of collagen and other organics in the mechanical properties of bone. *Osteoporosis Int.* 14 (5), S29–S36.
- Cusack, S., Miller, A., 1979. Determination of the elastic constants of collagen by Brillouin light scattering. *J. Mol. Biol.* 135, 39–51.
- Ding, M., Hvid, I., 2000. Quantification of age-related changes in the structure model type and trabecular thickness of human tibial cancellous bone. *Bone* 26, 291–295.
- Dormieux, L., Molinari, A., Kondo, D., 2002. Micromechanical approach to the behavior of poroelastic materials. *J. Mech. Phys. Solids* 50, 2203–2231.
- Eckardt, I., Hein, H.-J., 2001. Quantitative measurements of the mechanical properties of human bone tissues by scanning acoustic microscopy. *Ann. Biomed. Eng.* 29, 1043–1047.
- Eppel, M., 2001. Solid-state chemical methods to investigate the nature of calcified deposits. *Z. Kardiol.* 90 (Suppl. 3), III/64–III/67.
- Eppell, S., Tong, W., Katz, J., Kuhn, L., Glimcher, M., 2001. Shape and size of isolated bone mineralites measured using atomic force microscopy. *J. Orthopaed. Res.* 19, 1027–1034.
- Eshelby, J., 1957. The determination of the elastic field of an ellipsoidal inclusion, and related problems. *Proc. R. Soc. London, Ser. A* 241, 376–396.
- Fedorov, F., 1968. Theory of Elastic Waves in Crystals. Plenum Press, New York.
- Frasca, P., Harper, R., Katz, J., 1977. Collagen fiber orientations in human secondary osteons. *Acta Anatomica* 98 (1), 1–13.
- Fratzl, P., Fratzl-Zelman, N., Klaushofer, K., Vogl, G., Koller, K., 1991. Nucleation and growth of mineral crystals in bone studied by small-angle X-ray scattering. *Calcified Tissue Int.* 48, 407–413.
- Fratzl, P., Schreiber, S., Klaushofer, K., 1996. Bone mineralization as studied by small-angle X-ray scattering. *Connective Tissue Res.* 34 (4), 247–254.
- Fritsch, A., Dormieux, L., Hellmich, C., 2006. Porous polycrystals built up by uniformly and axisymmetrically oriented needles: homogenization of elastic properties. *C. R. Méc.* 334, 151–157.
- Frost, H., 1962. Measurement of osteocytes per unit volume and volume components of osteocytes and canaliculae (sic) in man. *Henry Ford Hospital Med. Bull.* 8, 208–211.
- Gebhardt, W., 1906. Über funktionell wichtige Anordnungsweisen der feineren und gröberen Bauelemente des Wirbeltierknochens [On the

- functionally important arrangements of the finer and coarser components of vertebrate bone]. *Archiv für Entwicklungs. Org.* 20, 187–322 (in German).
- Gilmore, R., Katz, J., 1982. Elastic properties of apatites. *J. Mater. Sci.* 17, 1131–1141.
- Giraud-Guille, M., 1988. Twisted plywood architecture of collagen fibrils in human compact bone osteons. *Calcified Tissue Res.* 42, 167–180.
- Gong, J., Arnold, J., Cohn, S.H., 1964. Composition of trabecular and cortical bone. *Anat. Rec.* 149, 325–332.
- Gould, S., Lewontin, R., 1979. The spandrels of San Marco and the Panglossian paradigm: a critique of the adaptionist program. *Proc. R. Soc. London, Ser. B* 205 (1161), 581–598.
- Hall, R., 1951. Variations with pH of the tensile properties of collagen fibres. *J. Soc. Leather Trades Chem.* 35, 195–210.
- Harley, R., James, D., Miller, A., White, J., 1977. Phonons and the elastic moduli of collagen and muscle. *Nature* 267, 285–287.
- Hasegawa, K., Turner, C., Burr, D., 1994. Contribution of collagen and mineral to the elastic anisotropy of bone. *Calcified Tissue Int.* 55, 381–386.
- Hassenkam, T., Fantner, G., Cutroni, J., Weaver, J., Morse, D., Hansma, P., 2004. High-resolution AFM imaging of intact and fractured trabecular bone. *Bone* 35, 4–10.
- Hellmich, C., 2005. Microelasticity of bone. In: Dormieux L., Ulm F.-J. (Eds.), *CISM Courses and Lectures*, vol. 480. Applied Micromechanics of Porous Media. Springer, Wien, New York, pp. 289–332.
- Hellmich, C., Ulm, F.-J., 2001. Hydroxyapatite is uniformly concentrated in the extracollagenous ultrastructure of mineralized tissue. In: Middleton, J., Shrive, N., Jones, M. (Eds.), *Proceedings of the Fifth International Symposium on Computer Methods in Biomechanics and Biomedical Engineering*, Rome, Italy.
- Hellmich, C., Ulm, F.-J., 2002a. Are mineralized tissues open crystal foams reinforced by crosslinked collagen?—some energy arguments. *J. Biomech.* 35, 1199–1212.
- Hellmich, C., Ulm, F.-J., 2002b. A micromechanical model for the ultrastructural stiffness of mineralized tissues. *J. Eng. Mech. (ASCE)* 128 (8), 898–908.
- Hellmich, C., Ulm, F.-J., 2003. Average hydroxyapatite concentration is uniform in extracollagenous ultrastructure of mineralized tissue. *Biomech. Modeling Mechanobiol.* 2, 21–36.
- Hellmich, C., Barthélémy, J.-F., Dormieux, L., 2004a. Mineral-collagen interactions in elasticity of bone ultrastructure—a continuum micromechanics approach. *European J. Mech. A—Solids* 23, 783–810.
- Hellmich, C., Ulm, F.-J., Dormieux, L., 2004b. Can the diverse elastic properties of trabecular and cortical bone be attributed to only a few tissue-independent phase properties and their interactions?—Arguments from a multiscale approach. *Biomech. Modeling Mechanobiol.* 2, 219–238.
- Hellmich, C., Ulm, F.-J., 2005a. Drained and undrained poroelastic properties of healthy and pathological bone: a poro-micromechanical investigation. *Transp. Porous Media* 58, 243–268.
- Hellmich, C., Ulm, F.-J., 2005b. Micro-porodynamics of bones: prediction of the ‘Frenkel-Biot’ slow compressional wave. *J. Eng. Mech. (ASCE)* 131 (9), 918–927.
- Hershey, A., 1954. The elasticity of an isotropic aggregate of anisotropic cubic crystals. *J. Appl. Mech. (ASME)* 21, 236–240.
- Hill, R., 1963. Elastic properties of reinforced solids: some theoretical principles. *J. Mech. Phys. Solids* 11, 357–362.
- Hodge, A., Petruska, J., 1963. Recent studies with the electron microscope on ordered aggregates of the tropocollagen molecule. In: Ramachandran, G. (Ed.), *Aspects of Protein Structure—Proceedings of a Symposium held in Madras 14–18 January 1963 and organized by the University of Madras, India*. Academic Press, London and New York, pp. 289–300.
- Hofstetter, K., Hellmich, C., Eberhardsteiner, J., 2005a. Development and experimental validation of a continuum micromechanics model for the elasticity of wood. *Eur. J. Mech. A—Solids* 24 (6), 1030–1053.
- Hofstetter, K., Hellmich, C., Eberhardsteiner, J., 2005b. Predicting wood strength from composition and microstructure: development and experimental verification of a continuum micromechanics model. In: Dormieux, L. (Ed.), *Proceedings of ‘Colloque Microstructure et Propriétés des Matériaux’*. Presses de L’École Nationale des Ponts et Chaussées. Marne-la-Vallée, France, pp. 217–222.
- Hollister, S., Fyhrie, D., Jepsen, K., Goldstein, S., 1991. Application of homogenization theory to the study of trabecular bone mechanics. *J. Biomech.* 24, 825–839.
- Hollister, S., Brennan, J., Kikuchi, N., 1994. A homogenization sampling procedure for calculating trabecular bone effective stiffness and tissue level stress. *J. Biomech.* 27 (4), 433–444.
- Hunt, B., Eipsman, R., Rosenberg, J., 2001. *A Guide to MATLAB for Beginners and Experienced Users*, first ed. Cambridge University Press, Cambridge, UK.
- Hunter, G., Hauschka, P., Poole, A., Rosenberg, L., Goldberg, H., 1996. Nucleation and inhibition of hydroxyapatite formation by mineralized tissue proteins. *Biochem. J.* 317, 59–64.
- Huo, B., 2005. An inhomogeneous and anisotropic constitutive model of human dentin. *J. Biomech.* 38, 587–594.
- Jäger, I., Fratzl, P., 2000. Mineralized collagen fibrils: a mechanical model with a staggered arrangement of mineral particles. *Biophys. J.* 79, 1737–1746.
- Jäger, C., Welzel, T., Meyer-Zaika, W., Eppe, M., 2006. A solid-state NMR investigation of the structure of nanocrystalline hydroxyapatite. *Magn. Reson. Chem.* 44 (6), 573–580.
- Katz, J., 1980. Anisotropy of Young’s modulus of bone. *Nature* 283, 106–107.
- Katz, J., 1981. Composite material models for cortical bone. *American Society of Mechanical Engineers*, New York, NY, USA, pp. 171–184.
- Katz, E., Li, S.-T., 1973. Structure and function of bone collagen fibrils. *J. Mol. Biol.* 80, 1–15.
- Katz, J., Ukraincik, K., 1971. On the anisotropic elastic properties of hydroxyapatite. *J. Biomech.* 4, 221–227.
- Katz, J., Yoon, H., Lipson, S., Maharidge, R., Meunier, A., Christel, P., 1984. The effects of remodelling on the elastic properties of bone. *Calcified Tissue Int.* 36, S31–S36.
- Katz, J., Bummerraj, S., Dreyfuss, J., Wang, Y., Spencer, P., 2001. Micromechanics of the dentin/adhesive interface. *J. Biomed. Mater. Res. B* 58, 366–371.
- Khuri-Yakub, B., 1993. Scanning acoustic microscopy. *Ultrasonics* 31 (5), 361–372.
- Knothe Tate, M., 2003. Whither flows the fluid in bone?—an osteocyte’s perspective. *J. Biomech.* 36, 1409–1424.
- Kotha, S., Guzelsu, N., 2003. Effect of bone mineral content on the tensile properties of cortical bone: experiments and theory. *J. Biomech. Eng.* 125, 785–793.
- Kreher, W., 1990. Residual stresses and stored elastic energy of composites and polycrystals. *J. Mech. Phys. Solids* 38 (1), 115–128.
- Kreher, W., Molinari, A., 1993. Residual stresses in polycrystals as influenced by grain shape and texture. *J. Mech. Phys. Solids* 41 (12), 1955–1977.
- Landis, W., Song, M., Leith, A., McEwen, L., McEwen, B., 1993. Mineral and organic matrix interaction in normally calcifying tendon visualized in three dimensions by high-voltage electron microscopic tomography and graphic image reconstruction. *J. Struct. Biol.* 110, 39–54.
- Landis, W., Librizzi, J., Dunn, M., Silver, F., 1995. A study of the relationship between mineral content and mechanical properties of turkey gastrocnemius tendon. *J. Bone Mineral Res.* 10, 859–867.
- Landis, W., Hodgins, K., Song, M., Arena, J., Kiyonaga, S., Marko, M., Owen, C., McEwen, B., 1996. Mineralization of collagen may occur on fibril surfaces: evidence from conventional and high-voltage electron microscopy and three-dimensional imaging. *J. Struct. Biol.* 117, 24–35.
- Lang, T., Keyak, J., Heitz, M., Augat, P., Lu, Y., Mathur, A., Genant, H., 1997. Volumetric quantitative computed tomography of the proximal femur: Precision and relation to bone strength. *Bone* 21 (1), 101–108.
- Lang, T., Guglielmi, G., van Kuijk, C., de Serio, A., Cammisia, M., Genant, H., 2002. Measurement of bone mineral density at the spine and proximal femur by volumetric quantitative computed tomography

- and dual-energy X-ray absorptiometry in elderly women with and without vertebral fractures. *Bone* 30 (1), 247–250.
- Laws, N., 1977. The determination of stress and strain concentrations at an ellipsoidal inclusion in an anisotropic material. *J. Elasticity* 7 (1), 91–97.
- Lees, S., 1987. Considerations regarding the structure of the mammalian mineralized osteoid from viewpoint of the generalized packing model. *Connective Tissue Res.* 16, 281–303.
- Lees, S., Cleary, P., Heeley, J., Garipey, E., 1979a. Distribution of sonic plesio-velocity in a compact bone sample. *J. Acoust. Soc. Am.* 66 (3), 641–646.
- Lees, S., Heeley, J., Cleary, P., 1979b. A study of some properties of a sample of bovine cortical bone using ultrasound. *Calcified Tissue Int.* 29, 107–117.
- Lees, S., Ahern, J., Leonard, M., 1983. Parameters influencing the sonic velocity in compact calcified tissues of various species. *J. Acoust. Soc. Am.* 74 (1), 28–33.
- Lees, S., Bonar, L., Mook, H., 1984a. A study of dense mineralized tissue by neutron diffraction. *Int. J. Biol. Macromol.* 6, 321–326.
- Lees, S., Pineri, M., Escoubes, M., 1984b. A generalized packing model for type I collagen. *Int. J. Biol. Macromol.* 6, 133–136.
- Lees, S., Tao, N.-J., Lindsay, M., 1990. Studies of compact hard tissues and collagen by means of Brillouin light scattering. *Connective Tissue Res.* 24, 187–205.
- Lees, S., Hanson, D., Page, E., Mook, H., 1994a. Comparison of dosage-dependent effects of beta-aminopropionitrile, sodium fluoride, and hydrocortisone on selected physical properties of cortical bone. *J. Bone Mineral Res.* 9 (9), 1377–1389.
- Lees, S., Probst, K., Ingle, V., Kjoller, K., 1994b. The loci of mineral in turkey leg tendon as seen by atomic force microscope and electron microscopy. *Calcified Tissue Int.* 55, 180–189.
- Lees, S., Hanson, D., Page, E., 1995. Some acoustical properties of the otic bones of a fin whale. *J. Acoust. Soc. Am.* 99 (4), 2421–2427.
- Lemons, R., Quate, C., 1974. Acoustic microscope—scanning version. *Appl. Phys. Lett.* 24 (4), 163–165.
- Lemons, R., Quate, C., 1975. Acoustic microscopy: biomedical applications. *Science* 188, 905–911.
- Levin, V., Michelitsch, T., Sevostianov, I., 2000. Spheroidal inhomogeneity in a transversely isotropic piezoelectric medium. *Arch. Appl. Mech.* 70, 673–693.
- Lorenzo, A., Caffarena, E., 2005. Elastic properties, Young's modulus determination and structural stability of the tropocollagen molecule: a computational study by steered molecular dynamics. *Med. Eng. Phys.* 38 (7), 1527–1533.
- Mammone, J., Hudson, S., 1993. Micromechanics of bone strength and failure. *J. Biomech.* 26, 439–446.
- Marotti, G., 1993. A new theory of bone lamellation. *Calcified Tissue Int.* 53 (Suppl. 1), s47–s56.
- Martin, R., Burr, D., Sharkey, N., 1998. *Skeletal Tissue Mechanics*. Springer, New York.
- Mayr, E., 1997. *This is Biology—The Science of the Living World*, first ed. Harvard University Press, Cambridge, MA, USA.
- McCarthy, R., Jeffcott, L., McCartney, R., 1990. Ultrasound speed in equine cortical bone: effects of orientation, density, porosity and temperature. *J. Biomech.* 23 (11), 1139–1143.
- Miller, A., 1984. Collagen: the organic matrix of bone. *Philos. Trans. R. Soc. London Ser. B* 304, 455–477.
- Mori, T., Tanaka, K., 1973. Average stress in matrix and average elastic energy of materials with misfitting inclusions. *Acta Metallurgica* 21 (5), 571–574.
- Morris, M., Lopez-Curato, J., Hughes, S., An, K., Bassingthwaite, J., Kelly, P., 1982. Fluid spaces in canine bone and marrow. *Microvascular Res.* 23, 188–200.
- Müller, R., Hahn, M., Vogel, M., Dellling, G., Rüggesegger, P., 1996. Morphometric analysis of noninvasively assessed bone biopsies: comparison of high-resolution computed tomography and histologic sections. *Bone* 18 (3), 215–220.
- Neu, C., Manz, F., Rauch, F., Merkel, A., Schoenau, E., 2001. Bone densities and bone size at the distal radius in healthy children and adolescents: a study using peripheral quantitative computed tomography. *Bone* 28 (2), 227–232.
- Nowlan, N., Prendergast, P., 2005. Evolution of mechanoregulation of bone growth will lead to non-optimal bone phenotypes. *J. Theor. Biol.* 235, 408–418.
- Peters, F., Schwarz, K., Eppe, M., 2000. The structure of bone studied with synchrotron X-ray diffraction, X-ray absorption spectroscopy and thermal analysis. *Thermochim. Acta* 361, 131–138.
- Pidaparti, R., Chandran, A., Takano, Y., Turner, C., 1996. Bone mineral lies mainly outside the collagen fibrils: predictions of a composite model for osteonal bone. *J. Biomech.* 29 (7), 909–916.
- Probst, K., Lees, S., 1996. Visualization of crystal-matrix structure. In situ demineralization of mineralized turkey leg tendon and bone. *Calcified Tissue Int.* 59, 474–479.
- Qin, Q.-H., Swain, M., 2004. A micro-mechanics model of dentin mechanical properties. *Biomaterials* 25, 5081–5090.
- Raspani, M., Guizzardi, S., Stocchi, R., Ruggeri, A., 1995. Different fibrillar architectures coexisting in Haversian bone. *Italian. J. Anat. Embryol.* 100 (Suppl. 1), 103–112.
- Raspani, M., Guizzardi, S., Stocchi, R., Ruggeri, A., 1996. Collagen fibril patterns in compact bone: preliminary ultrastructural observations. *Acta Anatomica* 155, 249–256.
- Reid, S., 1986. A study of lamellar organization in juvenile and adult human bone. *Anat. Embryol.* 174, 329–338.
- Rho, J.-Y., Kuhn-Spearing, L., Zioupos, P., 1998. Mechanical properties and the hierarchical structure of bone. *Med. Eng. Phys.* 20, 92–102.
- Rietbergen, B.v., Weinans, H., Huiskes, R., Odgaard, A., 1995. A new method to determine trabecular bone elastic properties and loading using micromechanical finite-element models. *J. Biomech.* 28, 69–81.
- Riggs, C., Vaughan, L., Evans, G., Lanyon, L., Boyde, A., 1993. Mechanical implications of collagen fibre orientation in cortical bone of the equine radius. *Anat. Embryol.* 187, 239–248.
- Rubin, M., Jasiuk, I., Taylor, J., Rubin, J., Ganey, T., Apkarian, R., 2003. TEM analysis of the nanostructure of normal and osteoporotic bone. *Bone* 33, 270–282.
- Rubin, M., Rubin, J., Jasiuk, I., 2004. SEM and TEM study of the hierarchical structure of C57BL/6J and C3H/HeJ mice trabecular bone. *Bone* 35, 11–20.
- Sasaki, N., 1991. Orientation of mineral in bovine bone and the anisotropic mechanical properties of plexiform bone. *J. Biomech.* 24, 57–61.
- Sasaki, N., Odajima, S., 1996a. Elongation mechanism of collagen fibrils and force-strain relations of tendon at each level of structural hierarchy. *J. Biomech.* 29 (9), 1131–1136.
- Sasaki, N., Odajima, S., 1996b. Stress-strain curve and Young's modulus of a collagen molecule as determined by the X-ray diffraction technique. *J. Biomech.* 29 (5), 655–658.
- Sasaki, N., Tagami, A., Goto, T., Taniguchi, M., Nakata, M., Hikichi, K., 2002. Atomic force microscopic studies on the structure of bovine femoral cortical bone at the collagen fibril-mineral level. *J. Mater. Sci. Materials in Medicine* 13 (3), 333–337.
- Seilacher, A., 1970. Arbeitskonzept zur Konstruktionsmorphologie [Concept for structure-morphology]. *Lethaia* 3, 393–396 (in German).
- Sevostianov, I., Kachanov, M., 2000. Impact of the porous microstructure on the overall elastic properties of the osteonal cortical bone. *J. Biomech.* 33, 881–888.
- Sietsema, W., 1995. Animal models of cortical porosity. *Bone* 17 (4), 297S–305S.
- Su, X., Sun, K., Landis, W., 2003. Organization of apatite crystals in human woven bone. *Bone* 32, 150–162.
- Suquet, P. (Ed.), 1997. *Continuum Micromechanics*. Springer, Wien, New York.
- Tai, K., Qi, H., Ortiz, C., 2005. Effect of mineral content on the nanoindentation properties and nanoscale deformation mechanisms of bovine tibial cortical bone. *J. Mater. Sci.: Materials in Medicine* 16, 947–959.

- Tong, W., Glimcher, M., Katz, J., Kuhn, L., Eppell, S., 2003. Size and shape of mineralities in young bovine bone measured by atomic force microscopy. *Calcified Tissue Int.* 72, 592–598.
- Torabia, S., 2004. Identification of a relationship between the chemical constituents of mineralized tissues: bridging computed tomography and micromechanical modeling, for noninvasive determination of elastic properties of bone. Master's Thesis, Vienna University of Technology.
- Torabia, S., Hellmich, C., 2004. In-vivo determination of elastic properties of bone, based on (p)QCT and micromechanical modeling. In: Laugier, P., Hans, D. (Eds.), *Proceedings of the 16th International Bone Densitometry Workshop*. Annecy, France.
- Turner, C., Cowin, S., Rho, J., Ashman, R., Rice, J., 1990. The fabric dependence of the orthotropic elastic constants of cancellous bone. *J. Biomech.* 23 (6), 549–561.
- Urist, M., DeLange, R., Finerman, G., 1983. Bone cell differentiation and growth factors. *Science* 220, 680–686.
- Vesentini, S., Fitić, C., Montecvecchi, F., Redaelli, A., 2005. Molecular assessment of the plastic properties of collagen-like homotrimer sequences. *Biomech. Modeling Mechanobiol.* 3, 224–234.
- Wachter, N., Augat, P., Mentzel, M., Sarkar, M., Krischak, G., Kinzl, L., Claes, L., 2001. Predictive value of bone mineral density and morphology determined by peripheral quantitative computed tomography for cancellous bone strength of the proximal femur. *Bone* 28 (1), 133–139.
- Wakashima, K., Tsukamoto, H., 1991. Mean-field micromechanics model and its application to the analysis of thermomechanical behaviour of composite materials. *Mater. Sci. Eng. A* 146 (1–2), 291–316.
- Wang, X., Qian, C., 2006. Prediction of microdamage formation using a mineral-collagen composite model. *J. Biomech.* 39, 595–602.
- Weiner, S., Wagner, H., 1998. The material bone: structure—mechanical function relations. *Annu. Rev. Mater. Sci.* 28, 271–298.
- Weiner, S., Arad, T., Sabanay, I., Traub, W., 1997. Rotated plywood structure of primary lamellar bone in the rat: orientation of the collagen fibril arrays. *Bone* 20, 509–514.
- Yoon, H., Katz, J., 1976. Ultrasonic wave propagation in human cortical bone—II. Measurements of elastic properties and microhardness. *J. Biomech.* 9, 459–464.
- Yu, Z., Boseck, S., 1995. Scanning acoustic microscopy and its applications to material characterization. *Rev. Mod. Phys.* 67 (4), 863–891.
- Zaoui, A., 1997. Structural morphology and constitutive behavior of microheterogeneous materials. In: Suquet, P. (Ed.), *Continuum micromechanics*. Springer, Wien, New York, pp. 291–347.
- Zaoui, A., 2002. Continuum micromechanics: survey. *J. Eng. Mech. (ASCE)* 128 (8), 808–816.
- Zaue, R., Yeni, Y., Bay, B., Dong, X., Fyhrie, D., 2006. Comparison of the linear finite element prediction of deformation and strain of human cancellous bone to 3D digital volume correlation measurements. *J. Biomech. Eng.* 128, 1–6.
- Zhang, D., Weinbaum, S., Cowin, S., 1998. Estimates of the peak pressures in pore water. *J. Biomech. Eng.* 120 (December 1998), 697–703.
- Zylberberg, L., Traub, W., deBuffrenil, V., Allizard, F., Arad, T., Weiner, S., 1998. Rostrum of a toothed whale: ultrastructural study of a very dense bone. *Bone* 23, 241–247.